Relationship between weather regimes and atmospheric rivers in East Antarctica.

Benjamin Pohl, Vincent Favier, Jonathan Wille, Danielle G. Udy, Tessa R. Vance, Julien Pergaud, Niels Dutrievoz, Juliette Blanchet, Christoph Kittel, Charles Amory, et al.

Relationship between weather regimes and atmospheric rivers in East Antarctica

Benjamin Pohl[1]*; Vincent Favier[2]; Jonathan Wille[2]; Danielle G Udy[3,4]; Tessa R Vance[5]; Julien Pergaud[1]; Niels Dutrievoz[2]; Juliette Blanchet[2]; Christoph Kittel[6]; Charles Amory[2,6]; Gerhard Krinner[2]; Francis Codron[7]

1 Biogéosciences, UMR6282 CNRS / Université de Bourgogne Franche-Comté, Dijon, France
2 Université Grenoble Alpes/CNRS/IRD/G-INP, IGE, Grenoble, France
3 Institute for Marine and Antarctic Studies, University of Tasmania, Hobart, Tasmania, Australia
4 ARC Centre of Excellence for Climate Extremes, University of Tasmania, Hobart, Tasmania, Australia
5 Australian Antarctic Program Partnership, Institute for Marine and Antarctic Studies, University of Tasmania, Hobart, Tasmania, Australia
6 Laboratory of Climatology, Department of Geography, University of Liège, Liège, Belgium
7 Laboratoire d'Océanographie et du Climat: Expérimentations et Approches Numériques, LOCEAN, Sorbonne Université, IRD, CNRS, MNHN, Paris, France

Submitted to
JGR-Atmospheres
21 May 2021
Revised
27 September 2021
23 November 2021
Accepted
28 November 2021

*** Corresponding Author Address**
Benjamin Pohl — Laboratoire Biogéosciences
6 bvd. Gabriel — 21000 Dijon — FRANCE
(+33)380393821 | benjamin.pohl@u-bourgogne.fr
https://orcid.org/0000-0002-9339-797X

Key Points

- Atmospheric Rivers reaching East Antarctica show strong association with synoptic weather regimes
- Atmospheric Rivers enhance the positive temperature and snowfall anomalies associated with the regimes
- Atmospheric Rivers occur when the synoptic configuration is anomalously strong over the Southern Ocean

Abstract

Here, we define weather regimes in the East Antarctica — Southern Ocean sector based on daily anomalies of 700hPa geopotential height derived from ERA5 reanalysis during 1979-2018. Most regimes and their preferred transitions depict synoptic-scale disturbances propagating eastwards off the Antarctic coastline. While regime sequences are generally short, their interannual variability is strongly driven by the polarity of the Southern Annular Mode (SAM). Regime occurrences are then intersected with atmospheric rivers (ARs) detected over the same region and period. ARs are equiprobable throughout the year, but clearly concentrate during regimes associated with a strong atmospheric ridges / blockings on the eastern part of the domain, which act to channel meridional advection of heat and moisture from the lower latitudes towards Antarctica.

Both regimes and ARs significantly shape climate variability in Antarctica. Regimes favorable to AR occurrences are associated with anomalously warm and humid conditions in coastal Antarctica and, to a lesser extent, the hinterland parts of the Antarctic plateau. These anomalies are strongly enhanced during AR events, with warmer anomalies and dramatically amplified snowfall amounts.

Large-scale conditions favoring AR development are finally explored. They show weak dependency to the SAM, but particularly strong atmospheric ridges / blockings over the Southern Ocean appear as the most favorable pattern, in which ARs can be embedded, and to which they contribute.

Key-Words

Atmospheric Rivers — Weather Regimes — East Antarctica — Temperature Anomalies — Snowfall amounts

1. Introduction

Although the Antarctic Ice Sheet (AIS) contribution to sea level rise is heavily influenced by ocean-driven mass loss (e.g., Edwards et al., 2019; Seroussi et al., 2020), the effects of sub-decadal to decadal precipitation variation on surface mass balance (SMB) dominate the overall mass balance variability of East Antarctica (IMBIE, 2018). A detailed understanding of SMB variability is therefore crucial to assess the future contribution of Antarctica to sea level rise (Seroussi et al., 2020). Uncertainties in future SMB changes contribute substantially to uncertainties in the projected Antarctic contribution to sea level rise, which varies between -7.8 cm and 43 cm sea level equivalent by 2100 under Representative Concentration Pathway (RCP) 8.5 scenario (Edwards et al., 2019, 2021; Seroussi et al., 2020). Estimates of regional scale SMB distribution and trends remain difficult to obtain as high-resolution data remain very scarce (e.g., Favier et al., 2017; Lenaerts et al., 2019). The strong variability of Antarctic SMB, both in time and space, further complicates this effort. Precipitation over most regions of Antarctica is controlled by a few high precipitation events (Turner et al. 2019). This characteristic has to be understood and correctly represented in models for accurate projections.

The strongly baroclinic Southern Ocean exhibits a high rate of cyclogenesis, and the southern Indian Ocean sector exhibits the highest frequency and strongest zone of cyclogenesis of the southern mid-latitudes (Simmonds et al., 2003). Yet, only a few of these cyclones actually reach the Antarctic coastline, and even fewer generate high precipitation events (Hoskins & Hodges, 2005; King & Turner, 2007; Simmonds et al., 2003; Turner et al., 2019; Uotila et al., 2013). These high precipitation events are generally recognized to occur when the mid-tropospheric jet configuration favors the development of atmospheric blocking ridges which direct heat and moisture transports further into the ice sheet (Hirasawa et al., 2013; Massom et al., 2004; Schlosser et al., 2010; Scott et al., 2019; Sinclair & Dacre, 2019). These blocking ridges have a particular prevalence in the Indo-Pacific sector due to a longitudinal SST gradient from the (colder) southeastern Indian Ocean to the (warmer) southwest Pacific sector (Pook, 1994; Pook et al., 2012). This region of blocking is of crucial importance to precipitation variability not only across East Antarctica (Massom et al., 2004), but also for the southern hemispheric nations of Australia and New Zealand (Pook et al., 2013; Pook et al., 2012; Risbey

et al., 2009; Udy et al., 2021). Blocking ridges are among various synoptic weather types that influence moisture transport and precipitation in the southern Indian Ocean region (Cohen et al., 2013; Udy et al., 2021). Synoptic-typing efforts are useful in identifying discrete atmospheric circulation patterns (e.g. Tozer et al., 2018; Pohl et al., 2021a) and of particular interest here, understanding which weather regimes provide the highest poleward moisture fluxes.

Recent research has categorized some of these particularly intense poleward moisture fluxes as atmospheric rivers (ARs), and connected them to high precipitation events across the AIS (Adusumilli et al., 2021; Gorodetskaya et al., 2014, 2020; Wille et al., 2021). Most research on ARs has focused on the mid-latitudes, but these weather systems also occur in Antarctica (e.g., Bozkurt et al., 2018; Gorodetskaya et al., 2014, 2020; Wille et al., 2019, 2021). ARs are elongated bands of strong horizontal moisture transport (Figure 1) typically embedded within a low-level jet ahead of an extratropical cyclone's cold front (Ralph et al., 2004; Zhu & Newell, 1998) and within the cyclone's warm conveyor belt (Dacre et al., 2019; Harrold, 1973; Madonna et al., 2014). Radiosonde observations during AR landfalls on the Antarctic coastline show extreme moisture, wind, and temperature values compared to the median state (Gorodetskaya et al., 2020). ARs have a distinctive integrated water vapor (IWV) profile on SSM/I (Special Sensor Microwave Imager) imagery (Ralph et al., 2017), but are more readily identified over polar regions using reanalysis IWV and integrated vapor transport (IVT) fields. The high moisture content within the AR is often related to moisture export from the lower latitudes, and is typically maintained through continuous and vigorous moisture convergence in the cyclone's warm conveyor belt and/or along the trailing cold front (Bao et al., 2006; Sodemann & Stohl, 2013). This connection with lower latitudes, along with atmospheric blocking or ridges directing the tropical moisture export poleward, contribute to differentiate ARs from non-AR related cyclones in regards to moisture transport.

While AR events are infrequent in Antarctica compared to other mid-latitude regions, they have a significant impact on SMB (Adusumilli et al., 2021; Gorodetskaya et al., 2014; Wille et al., 2019, 2021). Landfalls on the AIS occur between 1-3 times per year in a given region of Antarctica, yet are responsible for 10-20% of the annual snowfall budget across large swaths of East Antarctica (Wille et al., 2021). The AR fingerprint is more pronounced in high

precipitation events. ARs account for around 70% of the 1% most intense daily precipitation events (*ibid.*). Previous studies have demonstrated that high precipitation events control the interannual variability of surface snow accumulation (Gorodetskaya et al., 2014; Turner et al., 2019); annual AR frequency also controls the interannual variability of snow accumulation plus snowfall trends in many places of the AIS (Wille et al., 2021).

However, in addition to causing intense precipitation events, ARs can also cause strong melt events. They have triggered winter surface melt on the Antarctic Peninsula ice shelves along with being responsible for a majority of the summer melting events over Western Antarctic Ice sheet (WAIS) and the Ross ice shelf, especially in higher elevation regions (Adusumilli et al., 2021; Wille et al., 2019).

Overall, ARs have a predominantly positive impact on the AIS SMB and actively mitigate sea level rise driven from dynamic mass loss (Ligtenberg et al., 2013; Medley & Thomas, 2019; Wille et al., 2021). Mass gains from AR-related heavy snowfall occurrences across the AIS outweigh mass loss from sporadic AR-related melting events on the WAIS. How impacts from ARs on the AIS mass balance will change in the future is still uncertain. Indeed, any warming could increase melt and rain frequency over more areas of the continent (Wille et al., 2019; Kittel et al. 2021), with possible surface mass loss at lower elevations. Based on CMIP6 output, it is currently expected that the entire continent will warm between 1.3 ± 0.5°C (following the SSP1-2.6 forcing scenario) and 4.8 ± 1.2°C (SSP5-8.5) by the end of the 21st century (Bracegirdle et al., 2020).

In addition to further global warming increasing AR melt potential, there has been a general poleward shift in AR activity in conjunction with a poleward shift in the westerly jet over the past few decades (Espinoza et al., 2018; Ma et al., 2020). Meanwhile AR frequency has changed over certain regions of Antarctica during the satellite era with a decrease over parts of Adélie land, likely related to changes in atmospheric blocking occurrences around Antarctica (Wille et al., 2019, 2021). However, little is known on how AR tracks and impacts will change in a global warming context. This mainly stems from the lack of understanding of the synoptic weather regimes that transport these ARs towards the Antarctic coastline.

Here, we use a k-means clustering technique and an AR detection algorithm to analyze which synoptic weather regimes are most favorable for transporting ARs and their associated heat and moisture towards the East Antarctic coastline. Using both observations and reanalyses, we also assess the respective and combined influence of weather regimes and ARs on the climate of East Antarctica. Finally, we also attempt to separate, for each regime, the days associated with ARs from other ones, in order to identify possible factors that influence the development of AR events.

Section 2 gives a presentation of the climate conditions of East Antarctica and the data available to study it. Section 3 presents the methods used to define weather regimes and detect ARs. Section 4 characterizes synoptic-scale variability in the East Antarctica – Southern Ocean sector, and Section 5 presents the relationship between synoptic regimes and AR occurrence. The main results and their implications are finally summarized and discussed in Section 6.

2. Climate settings and available data

2.1 Climate settings

Long term meteorological surveys are available at the Dumont d'Urville (DDU) polar base (66°39'47"S, 140°00'03"E) since January 1956. The base is located on an archipelago, less than 5 km from the ice sheet boundary, and is characterized by the typical climatic conditions of the East Antarctic ice sheet (EAIS) coast. The average weather conditions (temperature: -10.8°C, pressure: 987.3 hPa, wind speed: 9.5 $m.s^{-1}$, preferential wind direction: 120-160°: König-Langlo et al. 1998) and seasonal conditions at the edge of the ice sheet play a fundamental role in snow accumulation, melting and the extent of pack ice close to the continent. Seasonality is characterized by a long winter, from May to October, a short summer, from November to January, and extremely short inter-seasons (Périard and Pettré 1993). The high seasonality of temperatures (-15°C in winter, -0.5°C in summer on average) implies that melting occurs only from December to February affecting snow conditions on the different nunataks as well as the break-up of sea ice around the archipelago. This is a direct

result of the variations in solar radiation energy input, strong in summer, and the "night-time" radiative cooling on the Antarctic plateau responsible for the establishment of stable atmospheric layers leading to the development of katabatic winds (Gallée and Pettré 1998; König-Langlo et al. 1998). The strong and persistent katabatic wind is a key characteristic of the climate of the region (Périard and Pettré 1993). The area is nevertheless affected by frequent low-pressure systems from the northwest (King and Turner 2007). More anticyclonic conditions are observed in summer and winter, but precipitation occurs throughout the year without a clear seasonal cycle (König-Langlo et al. 1998). Notable snow inputs are limited to a few heavy precipitation events that can occur at any time of the year (Turner et al. 2019). These are associated with warm and intense moisture transport from mid-latitudes, which can give rise to the rare rainfall events reported in the area (Favier et al., 2011). These events are expected to occur during atmospheric blocking conditions (Wille et al. 2021).

The weather conditions in the area are impacted by very high interannual climate variability which is expected to be related to large-scale atmospheric conditions (e.g., the intensity of the Southern Annular Mode: Marshall et al. 2017). However, the link between regional variability and large-scale circulation has never been thoroughly studied at the DDU polar base.

2.2 Data

Atmospheric fields used in this study are taken from the ERA5 ensemble reanalysis (C3S, 2017; Hersbach et al. 2020). ERA5 is the fifth generation of atmospheric reanalysis released by the European Center for Medium-Range Weather Forecasts. It currently covers the period 1979 onwards (with planned extension to 1950 onwards) and includes a 10-member ensemble to quantify uncertainties associated with the density and quality of the assimilated data. In this work, we use regular 0.25° x 0.25° grids of daily fields of the following variables: total water in the air column ($kg.m^{-2}$), air temperature at 2 m above the surface (T2m: °C), horizontal wind ($m.s^{-1}$), geopotential height (m) and specific humidity ($g.kg^{-1}$) at 700 hPa.

Global sea surface temperature fields (SST: °C) are taken from the ERSST v5 database (Huang et al. 2017) available at a monthly time step on a 2° x 2° global grid. This product is suited for

long-term and large-scale studies and is used here to analyze global teleconnections with our regimes.

Snowfall rates from the regional climate model (RCM) MAR in its latest Antarctic configuration (version 3.11; Kittel et al., 2021) without drifting-snow physics (Amory et al., 2021) were used in this study. The model was forced at its lateral boundaries, at the top of the atmosphere and at the ocean surface by 6-hourly ERA5 reanalysis and run at 35 km horizontal resolution over the Antarctic with a 120 second time step and outputs every three hours. The details of the simulation setup are given in Amory et al. (2021), based on the model version presented in Kittel et al. (2021). MAR is a hydrostatic model specifically designed to represent climate features typical of high-latitude regions such as the stable atmospheric boundary layer and its interactions with the snow-covered surface. In particular, the model accounts for the sublimation of precipitation in the lower troposphere, a process particularly active over the coastal margins of East Antarctica (Grazioli et al., 2017). MAR has been evaluated across the continent near-surface meteorological data (Mottram et al., 2021) and SMB (Agosta et al., 2019; Kittel et al., 2021) observations from the GLACIOCLIM-SAMBA quality-controlled dataset (Favier et al., 2013 updated by Wang et al., 2016) and in particular in the study area where a 157 km transect is surveyed annually (Agosta et al., 2012; Amory et al., 2021). Precipitation rates modelled by MAR have been used to demonstrate that ARs control the interannual variability of precipitation across Antarctica (Wille et al., 2021).

These datasets are supported by in-situ observations performed in Adélie Land by Météo-France, the French weather forecasting services. Daily data measured at the synoptic station of the DDU polar base are available since January 1956 and are used here over the period 1979-2018. For the present study, we make use of the following variables: daily minimum (Tn) and maximum (Tx) air temperature (°C), global surface radiation (RAD: $J.cm^{-2}$), mean sea-level pressure (SLP: hPa), wind speed ($m.s^{-1}$) and relative humidity (RH: %). Based on these series, diurnal thermal range (DTR, °C) has been calculated as Tx – Tn, and specific humidity (Q: $g.kg^{-1}$) has been computed using the Goff-Gratch equation based on vapor pressure (Goff and Gratch 1946). The number of available daily values for each variable is given in Section 5 below; from one variable to another, the fraction of missing values varies from 0.001% (for Tx) to 2.4% (for SLP and hence Q).

We also use the daily 2-m air temperature, surface pressure and wind speed data recorded by automated weather stations (AMRC-AWS) set up (1) on the D10 skyway, quite close to the DDU station (66.7°S, 139.8°E, 243 m asl, 5 km inland) available since January 1980, and (2) near Concordia station at Dome C (75.106°S, 123.346°E, 3250 m asl) available since February 1980. The time series collected at D10 have 33 to 39% of missing data, and their equivalents at Dome C from 7 to 8% (see Section 5.2).

Finally, we use a series of indices to monitor the polarity of the main modes of climate variability that could influence both the climate of the region, and the properties of our regimes and ARs. The state of ENSO is monitored through a spatially-averaged SST index computed over the Niño3.4 region (5°N-5°S, 170°W-120°W). The polarity of the SAM is derived from a daily index based on a Principal Component Analysis (PCA) of geopotential height anomalies south of 20°S. This index is mostly driven by geopotential height patterns over Antarctica [*Pohl and Fauchereau*, 2012; *Spensberger et al.*, 2020] and assumes that anomalies over the Southern Ocean display some zonal symmetry in the mid-latitudes. Hence, it could prove less relevant to analyze and interpret atmospheric features (i.e. weather regimes and AR events) located over the Southern Ocean over a longitudinally-bounded domain. Hence, we also considered an alternative index, computed as the normalized difference of daily SLP between Hobart, Australia (42.9°S, 147.3°E), and DDU. This index can be seen as a regional equivalent to the more zonally-symmetric, station-based SAM index proposed by Marshall (2003).

3. Methods

3.1 K-means clustering

Daily weather regimes are obtained through a k-means clustering (Cheng and Wallace 1993; Michelangeli et al. 1995). This algorithm is often used in climate science and has already been successfully used to decompose synoptic-scale meteorology in the Southern Hemisphere at subtropical (Fauchereau et al. 2009; Pohl et al. 2018), middle (Pohl et al. 2021a) and high

latitudes (Pohl and Fauchereau 2012; Richard et al. 2013). Alternative schemes of synoptic typing include self-organizing maps, as employed for a similar region by Udy et al. (2021), as well as PCA (Huth 1996; Pohl et al. 2009), or, more recently, archetypal analyses [*Risbey et al.*, 2021]. In the Southern Hemisphere, Pook et al. (2014) also performed a synoptic typing leading to differentiate frontal systems, cold-cored lows often leading to cut-off lows and warm-cored lows associated with the development of atmospheric ridges and troughs. Numerous classifications and/or tracking studies also exist for individual synoptic weather features, including extratropical cyclones [*Simmonds and Keay*, 2000; *Pezza et al.*, 2008; *Uotila et al.*, 2011; *Catto et al.*, 2015], anticyclones and blocking events [*Jones and Simmonds*, 1994; *Sinclair*, 1996; *Pezza and Ambrizzi*, 2003; *Liu et al.*, 2018; *Pepler et al.*, 2019b, 2019a].

Here, because our focus is primarily on lower-layer advections of moisture and temperature, the k-means clustering is applied to Z700 anomalies (after removing the mean annual cycle) taken from ERA5 reanalysis on the period 1 January 1979 to 31 December 2018 (i.e. 40 years of daily regimes). Regimes are calculated over the domain 45°S-75°S, 110°E-170°E (corresponding to 121 x 241 grid-points), which is approximately centered on Adélie land. This domain is chosen to match the typical size of synoptic perturbations and thus encompasses most of the disturbances that propagate in this sector. However, most regime representations are on a wider domain (30°S-85°S, 70°E-220°E: 221 x 601 grid-points), in order to show possible larger-scale patterns in which they could be embedded.

A PCA is applied to these Z700 anomalies prior to the k-means clustering to filter out atmospheric noise (i.e., smaller-scale features, or specificities of instantaneous fields that could make them deviate from the main atmospheric features most recurrently associated with similar synoptic contexts). The PCA-filtered Z700 anomalies account for 80% of the original variance in 5 eigenvectors. Following Michelangeli et al. (1995), the optimal number of clusters k is determined using a red-noise test, which compares the ‘‘classifiability’’ of real input data against Markov-generated red-noise data having the same covariance matrix. Results (Supp. Fig. 1) reveal that a partition into 15 regimes is the best possible choice.

3.2 AR detection scheme

To detect ARs in the Adélie land region, we employ the AR detection algorithm described in Wille et al. (2021). To summarize, this algorithm searches for grid cells between 37.5°S and 80°S where the meridional (v) component of integrated vapor transport (vIVT) exceeds the 98th percentile of all monthly vIVT values. The same is then done using integrated water vapor (IWV) to create a second catalog of AR detections. Using a relative threshold takes into account the progressive reduction of atmospheric saturation capacity moving poleward. Consecutive grid points above this relative threshold that extend at least 20° in the meridional direction are classified as ARs. Here, vIVT and IWV are defined as

$$vIVT = -\frac{1}{g}\int_{surface}^{TOA} qvdp, \quad (1)$$

$$IWV = -\frac{1}{g}\int_{surface}^{TOA} qdp, \quad (2)$$

where g (m.s^{-2}) is the gravitational acceleration, q (kg.kg^{-1}) is the specific humidity, v is the meridional wind velocity (m.s^{-1}), and p is the atmospheric pressure (hPa). vIVT and IWV are calculated on all reanalysis levels, from the surface to the top of atmosphere (TOA). The two detection schemes are used to retrieve ARs that make landfall along the coastline around DDU between 138°E - 142°E. The data used to initialize the AR detection is provided by the Modern-Era Retrospective analysis for Research and Applications, Version 2 (MERRA-2), which has a 0.5° x 0.625° horizontal resolution (Gelaro et al., 2017). Using MERRA-2 (i) is standard for all AR detection algorithms that are part of the Atmospheric River Tracking Method Intercomparison Project (ARTMIP; Rutz et al., 2019) , and (ii) ensure independence between the weather and AR definitions, both in terms of algorithms but also input dataset. Nonetheless, previous analysis has shown that when the AR detection algorithm is initialized with data from the ERA5 reanalysis, there is very little difference in AR detection frequency compared against MERRA-2 (Wille et al. 2021). The criteria for AR detection are stricter in this algorithm compared to global algorithms like Guan & Waliser (2015), as evidenced by the lower annual frequency of AR detections around the Antarctic coastline (1.2% and ~6% respectively; Wille et al. 2021). For a more detailed explanation of the AR detection algorithm, see Wille et al. (2021). An illustration of a typical AR event as detected by both IWV and vIVT schemes is given in Figure 1.

4. Characterization of the weather regimes over East Antarctica

4.1 Synoptic configurations

Figures 2 and 3 present the spatial anomaly patterns associated with the 15 weather regimes for selected mid-tropospheric, surface and vertically integrated variables. The regimes have been ordered by increasing longitude of associated positive 700 hPa geopotential height anomalies (Fig. 2). All regimes have quite similar sizes (from 795 days for regime #7 to 1213 days for #9). This is least partly attributable to the formulation of the k-means algorithm (Huth, 1996). The regime occurrences tend to show weak seasonality but large interannual variability (Supp. Fig. 2), a result similar to Udy et al. (2021) and Pohl et al. (2021a) over the Southern Ocean sector. The Z700 field, used as an input of the clustering analysis, is by construction well differentiated from one regime to another, especially on the inner region used for regime definition. All regimes tend to show wave-like alternations of positive and negative geopotential anomalies that strongly influence regional circulation anomalies in the troposphere. A few regimes show opposite-sign anomalies between Antarctica and the Southern Ocean (e.g., regimes # 5, 13 or 15), thereby suggesting potential interactions with the SAM (see Sect. 4.2) and/or strong associations with the SOM3 node of Udy et al. (2021; see also Supp. Table 2 and Supp. Figs. 21 to 23). However, most regimes correspond to wave patterns located over the Southern Ocean, north of the Antarctic coastline, with zonal extensions reminiscent of wavenumber 4-6 structures. This is fairly consistent with Udy et al. (2021). Regime sequences are generally short (generally less than 2 days, except for rare sequences exceeding 7 days and persisting up to 15 days: Supp. Fig. 3). Preferential transitions between regimes (Table 1) depict a clear tendency for eastward propagation of atmospheric configurations, most regimes being followed by regimes with quite similar patterns shifted to the east (Scarchilli et al. 2011; Udy et al. 2021; Pohl et al. 2021a). Taken together, these results suggest that these regimes mostly characterize synoptic-scale transient perturbations embedded in mid-latitude westerly circulation.

Regional atmospheric circulation adjusts to geopotential height anomalies through quasi-geostrophic lower-layer flux anomalies (Fig. 2). Anomalies of specific humidity at 700hPa (contours in Fig. 2), and total water content of the air column (contours in Fig. 3), are strongly coherent and directly modulated by meridional wind anomalies, with northerly fluxes advecting moist air from the lower latitudes while southerly fluxes advect dry air from the higher latitudes. There is also a very strong link with lower-layer air temperature anomalies, with northerly fluxes favoring anomalously warm conditions and southerly fluxes favoring anomalously cold conditions (colors in Fig. 3). Hence, the regimes are key for controlling mass, momentum and energy exchanges between the middle-latitudes of the Indo-Pacific sector and East Antarctica, a result confirming that of Udy et al. (2021).

To sum up, the 15 regimes identified here characterize the short-lived weather systems embedded in the mid-latitude westerlies that tend to propagate eastwards off the East Antarctica coast. By modulating meridional advections they strongly control exchanges between lower (subtropical to middle) and higher (polar) latitudes, resulting either in the ventilation of the polar air mass by warmer and moister air originating from the Southern Ocean, or symmetrically, intrusion of cold, dry air from the polar air mass in the middle latitudes.

4.2 Teleconnections with large-scale variability

The regimes defined here characterize the mid- to high-latitudes that connect the polar and tropical air masses. As a result, their occurrence and variability from one year to another could either relate to tropical or high-latitude modes of climate variability. Supplementary Figures 4 to 9 aim to assess the large-scale background conditions favoring regime occurrences, considering a 5% false discovery rate (Benjamini and Yekutieli 2001) for field significance assessment. These results are summarized in Table 2 for the two leading modes of climate variability in the tropical and polar latitudes of the Southern Hemisphere, i.e., El Niño Southern Oscillation (ENSO: McPhaden et al. 2006) and the SAM (e.g., Marshall 2003). No significant relationships were found with the Indian Ocean Dipole (not shown). As no significant trend is found in regime occurrences, the time series were not detrended in the following analyses. Preliminary tests (not shown) reveal that this does not qualitatively modify

our results, and none of the conclusions reached below is sensitive to this choice. This may be the case as the study period is too short to detect the low-frequency changes in the SH over the 20th century which were notable dominated by stratospheric ozone depletion (e.g., Marshall 2003; Renwick 2004; Thompson et al. 2011; Pohl and Fauchereau 2012, among many others).

Interannual correlations between seasonal regime occurrence and indices monitoring the polarity of these modes of variability (Table 2) reveal (i) a weak relationship with ENSO, a result that holds more generally for the whole SST field at tropical and middle latitudes (Supp. Figs. 8-9); (ii) a significant association with the SAM for 11 out of 15 regimes. Correlations generally tend to be stronger during the austral summer season (Supp. Figs. 4-5), and they are of consistent sign throughout the year. This relationship with the seasonal mean state of the SAM is responsible for the strong and significant correlation between weather regimes and Southern Ocean SST (Supp. Figs. 8-9). The positive phase of the SAM corresponds with a southward shift of the westerly wind circulation (e.g., Thompson and Wallace, 2000; Gillet et al., 2008; Fogt and Marshall, 2020), increases surface fluxes and northward Ekman transport and favoring anomalously cold SST (e.g., Lenton and Matear 2007).

In spite of such statistical significance, the strength of the relationship between the SAM and the occurrence of the regimes should not be overestimated as the teleconnection with the southern hemispheric Z700 field corresponds quite rarely to the canonical signature of the SAM, especially in winter (Supp. Figs. 4-5). Once the variability linearly related to the SAM is removed (Supp. Figs. 6-7), only smaller-scale signals remain significant, especially in the east hemisphere close to the domain used to define the regimes. This suggests a predominant, yet moderate association with the SAM, superimposed to more regional mechanisms; the latter, statistically independent of the SAM (at least at the seasonal scale), seem to relate to finer-scale perturbation in the circumpolar westerly circulation. In the Supplementary Materials, we also refine these results at the daily timescale, by considering synchronous associations between regime occurrences and the daily SAM index (Supp. Fig. 10). Results are broadly consistent with the seasonal timescale, that is, regime showing association with a given polarity of the SAM at the seasonal scale are preferentially associated with similar SAM polarities at the daily (intraseasonal and synoptic) scale. Strong variability and diversity are

nonetheless found within each regime, thereby weakening the relationship with the SAM. The SAM being a mode of much larger-scale than our regimes and ARs, we also consider a more regional index, consisting in the normalized difference of SLP between Hobart and DDU (Supp. Fig. 11). Results are very similar to those obtained with the daily SAM index, although smaller-scale atmospheric features like transient disturbances act to decorrelate both indices. Overall, these results at the seasonal and daily scale are strongly consistent (see Supp. Materials for details), and corroborate those of Udy et al. (2021).

5. Association with Atmospheric Rivers

5.1 Co-occurrence and modulation of AR properties

Here, the AR events identified by Wille et al. (2019; 2021) and reaching East Antarctica near DDU (between 138°E and 142°E: see Section 3.2) are extracted over the period 1979-2018, and their occurrences are intersected with those of the regimes discussed above. Results are displayed in Fig. 4, for each month of the year. While AR events are well distributed over the year, with nearly equal occurrences every month, they mostly coincide with 3 weather regimes (# 9, 10, 11). Some AR occurrences are also found for other regimes (especially, #7, 12, 13). These regimes are all characterized by positive geopotential height anomalies that are located off the coast of East Antarctica and channel northerly wind anomalies on their western flank towards the higher latitudes (Fig. 2). This results in anomalous warm and moist conditions along the western flank, an atmospheric signature that corresponds very well to the regional effects of AR events on the climate of Antarctica (Wille et al. 2021). Such a concentration of ARs in a limited number of regimes is less clear when considering the IWV detection scheme (Supp. Fig. 12), even if the hierarchy of the most favorable regimes for AR events is almost unchanged. In each case, the relationships between AR events and weather regimes remain stationary over the year, that is, they are not modulated by the annual cycle. These results clearly point out that the synoptic context has a strong influence on the occurrence and probability of AR events over the Southern Ocean region (a result that holds for the nodes obtained by Udy et al. (2021): Supplementary Materials).

Are the intrinsic characteristics of ARs (intensity, location and mean orientation) modified by the synoptic context, that is, are their attributes different from one regime to another? Figure 5 addresses this issue, and presents the statistical distributions of associated water vapor transport, the average longitude of AR patterns, and the average orientation of each AR, for the 5 most favorable regimes. Analyses are also duplicated for the 12 months of the year, in order to explore the seasonality of such AR properties. The orientation is computed here as Δlon/Δlat, with Δlat the difference in latitude between the northernmost point where the AR is detected and the latitude of DDU, and Δlon the longitudinal difference between these two same points. This simple metric approximates the angle of the AR over the oceanic part of the domain, i.e. before it reaches land and become more diffuse. Results for the IWV detection scheme are shown by Supp. Fig. 13. For both AR detection schemes, water vapor transport and AR mean longitude and orientation are all quite stable across the year (right-hand column), except for a weak tendency for austral spring events (occurring from September to November) to be associated with slightly weaker vapor transport. There is a large spread in the monthly distributions of AR attributes, which denotes strong diversity from one event to another. This indicates that ARs can occur (Fig. 4) and have roughly similar mean characteristics (Fig. 5) throughout the year. Water vapor transport associated with the AR events is also similar across regimes: the larger transport values found for regimes #7 and #13 should be considered with caution, since associated sample size is much smaller than for regimes #9-10-11 (Figs. 4-5).

As expected, weather regimes have a major influence on the location of ARs, with the mean longitude of the AR events coherent with the regime classification. The latter (increasing from one regime to another, as a consequence of the regime reordering by increasing longitudes of associated patterns: Figs. 2-3) corresponds well to the longitude of the southward advections found west of the anticyclonic ridge / blocks in the composite mean anomaly patterns associated with the regimes. Regimes also modify the orientation of ARs reaching DDU: regimes #7 and #9 are mostly associated with AR events oriented northwest to southeast, while the north-south direction prevails for regime #10 and #11. ARs display a marked northeast to southwest angle when co-occurring with regime #13; however, this contains fewer events (this regime being likely associated with ARs often reaching Antarctica further east). Results are consistent for both AR detection schemes. These results suggest that

(i) the synoptic configurations with marked northerly wind anomalies (likely to span from northwesterly to northeasterly from one AR to another) embedded in and located west of atmospheric ridges / blocks are the most favorable conditions for AR occurrence; (ii) that these ARs reaching the DDU sector could advect southwards moisture coming from a vast region, from the southern part of the Indian Ocean to the southwest Pacific sector near New Zealand. Further analysis is ongoing to assess the moisture sources of these ARs in detail.

5.2 Combined effects on the climate of East Antarctica

Figure 6 presents the anomalies of atmospheric variables measured at the synoptic weather station of DDU synchronous with the 15 regimes (corresponding climatologies are shown in Supp. Fig. 14). The weather regimes being based on geopotential height, strong regime-dependency is logically found in SLP. Regime effects are similar between the two opposite seasons of austral winter and summer (Supp. Figs. 15-16).

While diurnal thermal range is quite stable across regimes, the latter have a larger influence on air temperature, modulating daily minimum and maximum temperature in an almost similar way. Here, the sign of meridional wind anomalies is the key parameter that controls the sign of temperature anomalies along the coast: regimes favoring southerly anomalies from the hinterland, enhancing katabatic winds, lead to anomalously cold conditions at DDU (this is for instance the case for regimes # 3, 4, 5 and 15). Symmetrically, northerly advections clearly favor warm anomalies reaching DDU (e.g. regimes # 6, 10, 11), associated with larger local wind speeds. The role of synoptic regimes for modulating local-scale temperature may also be dampened by more local effects: this is the case for regime #9, which advects warmer air from the mid-latitudes west of the station, but circulation anomalies associated with anticyclonic conditions further east deflect the winds, with a marked westerly component over coastal Antarctica that enhances their residency time over land. This acts to weaken the temperature anomalies associated with this regime. The amplitude of temperature anomaly changes from one regime to another (typically ± 5°C) should be compared (i) to the total spread internal to each regime (typically, 5°C according to the inter-quartile range regrouping 50% of the days: see boxplots in Fig. 6) and (ii) the annual thermal range (roughly 15°C: Supp. Fig. 14). The effects of the regimes on air temperature anomalies are very similar in winter

and in summer (Supp. Figs. 15-16), albeit a much larger amplitude of the anomalies in winter. These results show that, while weather regimes significantly influence temperature variability according to analyses of variance (labels in Fig. 6), they only account for a limited fraction of the total variability. Residual variance internal to the regimes needs therefore to be considered for more detailed analyses (see Sect. 5.3).

Quite logically, the regimes associated with warm anomalies caused by advections from the Southern Ocean also transport moisture towards the DDU sector. This leads to stronger modulation of Q anomalies and weaker modulation of RH anomalies by the synoptic configurations, and hence the regimes. Q also shows much stronger seasonality than RH (Supp. Fig. 14). Yet, regime influence on air humidity is similar throughout the year (Supp. Figs. 15-16), the opposite seasons differing mostly in the larger amplitude of Q anomalies in summer. As expected for polar latitudes, surface solar radiation (RAD) is the variable showing the largest modulation by the annual cycle, with values close to zero in winter. Regimes appear to have a weak influence on RAD on average (Fig. 6), which logically increases in summer (Supp. Fig. 16). At that time, regimes associated with positive anomalies of Q clearly correspond to the most negative anomalies of RAD, presumably due to increased cloud cover. Counter-intuitively, these regimes are not associated with low-pressure anomalies in the DDU region, but tend to correspond to the regimes associated with the largest occurrence of AR events, such days contributing to the most negative RAD anomalies (even in winter: Figs. 6 and Supp. Figs. 15-16). AR days tend also to be anomalously windy and humid (especially for Q), and anomalously warm (during all seasons, and more particularly for Tx). While the concept of daily extrema is less meaningful in winter, the strong influence of ARs on Tx denotes abrupt warming events, mostly driven by strong and sudden advections of moisture and heat from the lower latitudes.

In order to disentangle the mean influence of synoptic conditions (materialized here by the regimes) on the local climate in DDU, from the specific effect of AR events, Fig. 6 is accompanied by Supp. Table 1 in the Supplementary Materials, that tests the significance of (i) local anomalies against the climatology during all regime occurrences, and (ii) local differences between AR and non-AR days within each regime. Results reveal that overall regime anomalies and differences between AR and non-AR days are not directly related. This

implies that the specific effects of ARs on the local weather are largely independent of the mean conditions that prevail at DDU during similar synoptic contexts. They also strongly depend on the considered meteorological variable. As far as the main AR-favorable regimes (#9-10-11) are concerned, most anomalies (against the climatology) and most differences (between AR and non-AR days) tend to be significant, except for AR influence on the diurnal thermal range and sea-level pressure.

Figure 7 presents similar analyses for meteorological variables (2-m air temperature, surface pressure and wind speed) measured at the D10 skiway station (5km away from the DDU synoptic station, on the mainland) and at Dome C, at about 1100km from the coastline. This interior site is also more elevated (3250m asl on an ice dome over the Antarctic plateau: Section 2.2). Corresponding seasonalities are shown in Supp. Fig. 17. D10 displays strong similarities with nearby DDU station, both in terms of seasonality and composite anomalies during regime and AR occurrences. By contrast, in Dome C, the annual cycle of temperature is much stronger, especially due to very cold conditions during the polar night. Surface pressure also shows some seasonal dependency (which is not the case for coastal stations), and wind speeds are much reduced compared to the katabatic wind regime recorded along the coast (Supp. Fig. 17). Weather regimes have limited influence on wind speed at Dome C, but AR days at DDU tend to coincide with the windiest days there (especially during the most favorable regimes, #9-10-11). They modulate surface pressure in a coherent and consistent way compared to D10 and DDU, indicative of large-scale signals with strong spatial coherence. Similar results hold for air temperature in Dome C, also responding to both regimes and coastal AR events consistently with DDU. In particular, regimes associated with northerly anomalies favor anomalously warm (that is, less cold) conditions in Dome C, a result further enhanced during AR events. This is consistent with the relatively larger wind speed during these days, which corresponds to strong advections of temperature and moisture from lower latitudes. These observations are consistent with reanalyses (Fig. 3), an issue further explored in section 5.3.

5.3 Interactions between regimes and ARs at regional scale

Here, we complement the local analyses presented in Section 5.2 at the regional scale, using reanalyses and regional climate simulations. Our goal is to identify the differences between AR and non-AR days within the same regime. This question leads us to analyze more in detail the residual variability occurring within weather regimes, and to determine if AR events can contribute to explain part of it.

Figure 8 presents normalized snowfall anomalies during the 5 regimes most favorable for ARs at DDU (namely, #7, 9, 10, 11, 13: Fig. 4; Supp. Fig. 12). The normalization is used to consider the strongly decreasing snowfall amounts from the coastal regions to the inland plateau (e.g., Turner et al., 2019). Supp. Fig. 18 complements these analyses by presenting the raw (non-normalized) anomalies during the occurrence of all 15 weather regimes. The regimes most frequently associated with ARs are among those that bring the largest snowfall amounts, especially along the coast (Supp. Fig. 18). The location of the largest amounts coincides well with the longitude of the northerly anomalies advecting moisture from the lower latitudes towards Antarctica (Figs. 2-3; Servettaz et al. 2020). In detail, however, these "snowy" regimes appear strongly driven by high accumulations recorded during a few AR events, while the large majority of days not associated with ARs exhibit much weaker snowfall (Fig. 8). This means that the "snowy" regimes are mostly snowy during ARs, and that a few AR days strongly influence the average amounts recorded during all regime occurrences agreeing with the analysis of AR-influence on high precipitation events on this region (e.g., Wille et al., 2021). The same conclusions hold for all 5 regimes, and for the coastal regions near DDU but also for Plateau regions like Dome C. There, snowfall amounts are lower, and working with non-normalized anomalies would suggest strongly decreasing AR influence towards the south. Moreover, a study at Dome C should consider the role of 'diamond dust' and hoar frost in net accumulation (e.g., Stenni et al., 2016, Schlosser et al., 2016, 2017). However, there are far fewer occurrences with relatively large daily totals, with significantly higher magnitude than what it is expected for diamond dust precipitation (e.g. Schlosser et al., 2017). Nonetheless, our results confirm that even far from the coast, ARs are responsible for a sizeable fraction of total snowfall amounts, despite their infrequent occurrence (Wille et al. 2021).

Such intra-regime diversity leads us to reinvestigate the composite mean anomaly patterns discussed above (Figs. 2-3) as the typical spatial signature of the regimes. Figure 9 duplicates the analyses of Figure 8 but for the geopotential height, horizontal wind and specific humidity at 700hPa derived from ERA5 reanalyses (thus giving results directly comparable to Fig. 2 but breaking down by AR and non-AR days at DDU). The AR detection scheme used here is vIVT: the results obtained using the IWV criterion are similar (Supp. Fig. 19). Figure 10 (complemented by Supp. Fig. 20 for the IWV detection scheme) shows similar analyses applied to anomalies of 2-m temperature and total water in the air column, as an equivalent of Fig. 3 including specific AR effects.

Whatever the regime considered, days associated with AR events significantly differ from other days. AR days generally correspond to synoptic configurations that are much stronger than other (non-AR) days. This is particularly true for the anticyclonic ridge / blocking (materialized in the figure by positive geopotential height anomalies) located northeast of the DDU region, and acting to deviate atmospheric fluxes, and thus in promoting meridional transport of heat and moisture towards that region (e.g., Massom et al. 2004; Irving and Simmons 2015). Through geostrophy, such enhanced blockings favor stronger moisture and heat transport, forming a favorable regional-scale configuration in which AR events can be embedded (and to which they can contribute). The southward transport of heat and atmospheric moisture associated with ARs is channeled by strong ridges / blocks located further east (Fig. 9). This explains the paradox of heavy precipitation occurring during high pressure and high wind conditions in coastal regions like DDU and D10 (Figs. 6-7). These amplified atmospheric fluxes yield strong extended warm anomalies over Antarctica that reach the plateau (Fig. 10). They also convey precipitable water in the air column, but humidity barely penetrates over the landmass due to orographic lifting along and near the coastline, bringing abundant snowfall there (Fig. 8; Servettaz et al. 2020). This explains why AR events at the coastline may affect Dome C (at about 1100km from the coast), as proposed by Schlosser et al. (2017) for the strongest blocking anticyclones, where they are associated with strong wind speeds and warm anomalies (Fig. 8; Supp. Fig. 18).

From the frequency labels of Figs. 9-10, it is clear that AR days only represent a very small proportion of all days ascribed to each of these AR favorable regimes. Such marked difference

in the number of days considered to perform the analyses of Figs. 9-10 raise two questions. (i) From a statistical point of view, could the significance of the differences between AR and non-AR days be altered by dissimilar sample sizes, or in other words, what is the statistical robustness of the differences identified in these figures? (ii) From a physical point of view, do all strong anticyclonic ridges / blocks lead to AR events, or are these anomaly patterns a necessary but not a sufficient condition for AR development? Table 3 attempts to address these issues, by analyzing how often positive geopotential height anomalies differ between AR and non-AR samples of days within each weather regime. The systematic or occasional significance of the differences is assessed by choosing randomly 100,000 samples of non-AR days within each regime, that have the same size as corresponding AR samples. Table 3 then presents the proportion of significance differences among these 100,000 samples, according to two-tailed t-tests at contrasted significance bounds. Here, these tests are applied to the regional maximum of positive geopotential height anomalies, identified as a robust descriptor of atmospheric centers of action associated with extra-tropical weather regimes by Pohl et al. (2021b). Results (Table 3) reveal that, for rather low significance levels (95%, i.e., $p=5x10^{-2}$), geopotential height anomalies are almost systematically larger during AR days, confirming the importance of strong ridges / blockings for poleward AR transport. Results are less clear at higher significance level (99.99%, i.e., $p=10^{-4}$). Here, the proportion of non-AR days that differ from AR days, while virtually unchanged for regime #10, drops to roughly 63-69% for regime #7 (depending on the AR detection scheme). For regime #9 the detection scheme has a dramatic influence (84% of statistically significant Max_Z differences for vIVT against only 17% for IWV). Regime #11 shows similar behavior. Regime #13 forms a noticeable exception, with much weaker proportion of significance differences between AR and non-AR days, whatever the detection scheme used. Caution is needed with this regime, because AR days are very rare (only 16 days over the 40-year long period: Fig. 9). This is probably because this regime yields AR events that reach Antarctica further east (through northwesterly or northerly anomalies), the case of northeasterly ARs remaining rather rare (Fig. 5).

Overall, these results suggest that some strong anticyclonic ridges / blocks may exist, even in the absence of ARs. From one regime to another, the fraction of strong geopotential maxima co-occurring with ARs is very dissimilar, which leads us to conclude that strong ridges / blocking are a necessary, but not a sufficient condition for AR development. These results

help identify the most favorable conditions leading to ARs. They also point out that weather regimes conceal strong internal variability, but their usefulness to identify the atmospheric configurations leading to climate extremes in Antarctica has been confirmed in this work, although other influences are also at play.

6. Discussion and Conclusion

Weather regimes obtained through k-means clustering have been defined over the East Antarctica / Southern Ocean sector based on daily maps of 700hPa geopotential height anomalies. These regimes depict the eastward propagation of transient perturbations embedded in the mid-latitude westerlies. Regime sequences are short, suggesting a strong association with the synoptic-scale variability. Nonetheless, interannual variability in regime occurrences is quite strong, and appears primarily driven by the phase of the SAM. These results tend to be stronger in austral summer.

Regime occurrences were then compared to atmospheric rivers (ARs) detected over the same domain and period by two complementary schemes based on contiguous patterns of anomalously strong integrated vapor transport or integrated water vapor in the air column between southern mid-latitudes and Antarctica. ARs show uniform distribution over the year but show strong preferential co-occurrence with regimes characterized by an atmospheric ridge / blocking located off the Antarctica coastline, and acting to favor meridional transport of heat and moisture from the lower latitudes to the polar regions. Such regimes are then associated, on average, with increased temperature and snowfall over Antarctica, but more detailed analysis reveals that such anomalies tend to be enhanced during AR events and much weaker (though still significant) the rest of the time. This is especially true for snowfall amounts and 2-m air temperature anomalies, dramatically amplified during AR days, as a consequence of southward transport from the middle to the high latitudes. Finally, we show that, within all regimes, days associated with ARs significantly differ from the composite mean. Generally, they correspond to stronger synoptic configurations, and especially, to stronger atmospheric ridges / blockings that are located to the northeast of the region most influenced by the corresponding ARs. One explanation for these enhanced downstream ridges

is the moisture export from the lower latitudes at the beginning of the AR life cycle condenses as the flow travels poleward over cooler sea surface temperatures. The condensation releases latent heat fueling cyclogenesis via differential diabatic heat and acts to decrease the potential vorticity of the downstream ridge (Madonna et al., 2014, Woolings et al., 2018, Terpstra et al., 2021). Although moisture sources still remain to be assessed, the large diversity in AR orientation, location and shape, suggests that moisture could mainly originate from a vast region spanning from the Indian Ocean to New Zealand, including thus the Great Australian Bight, Southwest Pacific Ocean and Tasman Sea. Anomalously strong ridge / blocking direct such moisture through northerly anomalies towards Antarctica. Along the coast, this leads to large snowfall accumulation, and the transport of heat from the lower latitudes can penetrate inland and yield warm anomalies more than 1000km from the coast. In these interior regions, snowfall rates are much lower, but still above average, during coastal AR events. However, moisture amounts released in the cold atmosphere of Dome C could partly contribute to clear-sky precipitation occurring later (e.g., Schlosser et al. 2017), but such effect has not been analyzed here, as the processes associated with diamond dust occurrences are largely missed in most models (e.g., van de Berg et al. 2005, Genthon et al. 2009, Souverijns et al. 2019).

These results help identify the regional-scale conditions favoring AR events, particularly strong synoptic configurations of the regimes associated with an atmospheric ridge / block located off the Adélie Land (East Antarctica) coastline. In order to differentiate between ridging / blocking, blocking indices like those developed by Pook and Gibson (1999) could be used as a complement to the analysis of the positive Z700 anomalies. However, strong ridge / blocks are likely to be a necessary but not a sufficient condition. This is probably true for the entire Antarctic coastline as an overall high zonal pressure difference between the upstream trough and downstream ridge coincides, but does not alone assure an AR landfall on the continent (Wille et al. 2021). The small number of ARs over the period should be compared to the size of their most favorable regimes (e.g., Fig. 8): within regimes #9, #10 and #11 (i.e. those associated with the largest occurrence of ARs), only 6.9%, 10.1% and 12.5% of the days correspond to AR events according to the vIVT detection scheme, respectively. For the IWV detection scheme, these values even drop to 2.8%, 8.7% and 6.0%. Hence, all strong blocks are not associated with AR events (as confirmed by analyses of random selection of non-AR

samples, that reveal that strongly variable proportions of strong ridges / blocks co-occur with AR events). There is therefore a strong need to better understand all mechanisms and processes that differentiate favorable conditions that are, and those that are not, associated with ARs.

Future work should be devoted to this issue. A better understanding and seamless forecasting of major AR events implies a more precise knowledge of their causes and intrinsic properties. Although this study clearly identified synoptic contexts / weather regimes favorable for AR occurrences, confirming the key role of intense anticyclonic ridging / blocking in the generation of intense warm and moist intrusions of marine air over the ice sheet (Scott et al. 2019), there is now a need to better differentiate the strong, quasi-stationary subpolar blocks, from other anticyclones and transient atmospheric ridges embedded in synoptic-scale disturbances and wave activity that cause precipitation variability and extreme events in southern hemispheric territories such as Australia and New Zealand (Pook et al., 2012; Udy et al., 2021). Large-scale wind shear in the middle latitudes upstream of the ridges / blocks could contribute to control the origin of the air particle, and therefore their heat and moisture content. Back-trajectories could be an efficient tool to explore this and identify sources of moisture export (e.g., Scarchilli et al., 2011, Sodemann & Stohl, 2013). At higher latitudes, the ventilation of the Antarctic air mass by northerly advections is likely to depend on the strength of the southerly katabatic winds. Horizontal pressure gradients between the landmass and the Southern Ocean could modulate the spatial extension of AR influence on the inland plateau: part of these gradients could be influenced by the state of the SAM, but many other factors could also be at play.

The results obtained here over Adélie and Victoria land point out a strong control of anticyclones on the location and orientation of AR events. Future work could attempt to analyze to which extent these results are zonally symmetric, that is, hold for other longitudes along the Antarctica coastline. Our results suggest that the mechanisms discussed here could be largely valid over most parts of East Antarctica (including remote regions of Wilkes, Enderby and Queen Maud lands) where the coastline and inland topography also show similarities with the region considered in this work, and strong zonal symmetry with relatively consistent annual AR frequencies along the coastline (Wille et al., 2021). Generalizing these

results for other longitudes is among the remaining open issues to be addressed. Last but not least, long-term changes in AR (e.g., Espinoza et al. 2018), weather regimes, and their interdependence, are among the major aspects of climate change that need to be explored for these regions. Here, long-term evolutions mostly involve the latitudinal dimension. Changes in the general circulation and especially the expected meridional shifts of the storm tracks (either driven by increasing greenhouse effect or ozone recovery: e.g., Thompson et al. 2011), low-frequency evolutions in the state of the SAM, and ongoing warming trends, could all modify the intrinsic properties of both regimes and AR events, that is, their recurrence, location (Ma et al. 2020), extension and intensity. Potentially, they could also change their effects on the ice sheet, e.g. through stronger extreme precipitation due to Clausius-Clapeyron scaling (Betts and Harshvardhan 1987; Trenberth et al. 2003; Pall et al. 2007; Kharin et al. 2007; O'Gorman and Schneider 2009; Muller et al. 2011; Westra et al. 2014), or through enhanced melt occurring under warmer surface air temperatures, especially near the coast (Wille et al. 2019). Because of their major influence for the climate of Antarctica, these issues certainly deserve further work from the scientific community.

Acknowledgments

The authors thank the JGR editorial staff, as well as Dr. James Risbey and two anonymous reviewers for their constructive comments that helped improve this work. They also thank Dr. Philip Reid who provided data managed by the Australian Bureau of Meteorology. This article is part of the ANR ARCA (Atmospheric River Climatology in Antarctica; grant number ANR-20-CE01-0013: https://anr.fr/Project-ANR-20-CE01-0013) funded by the French National Research Agency. All analyses were made with python (libraries numpy, pandas, scipy, sklearn, math, matplotlib, cartopy, seaborn, netCDF4), the developers of which are thanked. Calculations were performed using HPC resources from DNUM CCUB (Centre de Calcul de l'Université de Bourgogne).

CRediT authorship contribution statement

B Pohl: Conceptualization, Methodology, Software, Formal analysis, Visualization, Writing; **V Favier:** Conceptualization, Methodology, Writing, Resources, Funding acquisition; **J Wille:** Methodology, Software, Formal analysis, Visualization, Writing; **DG Udy:** Writing, Data curation; **TR Vance:** Writing, Data curation; **J Pergaud:** Data curation; **N Dutrievoz:** Writing; **J Blanchet:** Writing; **C Kittel:** Data curation, Writing; **C Amory:** Writing; **G Krinner:** Writing; **F Codron:** Writing

Data Availability Statement

ERA5 data can be retrieved from https://cds.climate.copernicus.eu/cdsapp#!/search?type=dataset&text=era5. ERSST data is available at https://psl.noaa.gov/data/gridded/data.noaa.ersst.v5.html. Météo-France performs the meteorological data from Dumont d'Urville, partly available at https://www.infoclimat.fr/observations-meteo/temps-reel/terre-adelie-dumont-d-urville/89642.html. Meteorological data recorded at other sites in Adelie land are accessible at http://pp.ige-grenoble.fr/pageperso/faviervi/observatory.php and http://amrc.ssec.wisc.edu/data/view-data.php?action=list&product=surface. Weather data at Hobart was provided by the Australian Bureau of Meteorology (http://www.bom.gov.au/climate/dwo/index.shtml). The SAM index was retrieved from https://www.cpc.ncep.noaa.gov/products/precip/CWlink/daily_ao_index/aao/aao.shtml. The Niño3.4 index was retreieved from https://climatedataguide.ucar.edu/climate-data/nino-sst-indices-nino-12-3-34-4-oni-and-tni. The MAR source code and outputs as used in this study can be found at https://zenodo.org/record/4314872. The MAR source code is tagged as v3.11.2 on https://gitlab.com/Mar-Group/MARv3.7: see http://www.mar.cnrs.fr for more information.

References

Adusumilli, S., Fish, M.A., Fricker, H.A., & Medley, B. (2021). Atmospheric River Precipitation Contributed to Rapid Increases in Surface Height of the West Antarctic Ice Sheet in 2019. Geophysical Research Letters, 48(5), e2020GL091076. https://doi.org/10.1029/2020GL091076

Agosta, C., Favier, V., Genthon, C. et al. (2012). A 40-year accumulation dataset for Adelie Land, Antarctica and its application for model validation. Clim Dyn 38, 75–86. https://doi.org/10.1007/s00382-011-1103-4

Agosta, C., Amory, C., Kittel, C., Orsi, A., Favier, V., Gallée, H., van den Broeke, M. R., Lenaerts, J. T. M., van Wessem, J. M., van de Berg, W. J., & Fettweis, X. (2019). Estimation of the Antarctic surface mass balance using the regional climate model MAR (1979–2015) and identification of dominant processes, The Cryosphere, 13, 281–296, https://doi.org/10.5194/tc-13-281-2019

Amory, C., Kittel, C., Le Toumelin, L., Agosta, C., Delhasse, A., Favier, V., & Fettweis, X. (2021). Performance of MAR (v3.11) in simulating the drifting-snow climate and surface mass balance of Adelie Land, East Antarctica, Geosci. Model Dev., 14, 3487–3510. https://doi.org/10.5194/gmd-14-3487-2021

Bao, J.-W., Michelson, S. A., Neiman, P. J., Ralph, F. M., & Wilczak, J. M. (2006). Interpretation of Enhanced Integrated Water Vapor Bands Associated with Extratropical Cyclones: Their Formation and Connection to Tropical Moisture. Monthly Weather Review, 134(4), 1063–1080. https://doi.org/10.1175/MWR3123.1

Benjamini, Y., and D. Yekutieli, 2001: The control of the false discovery rate in multiple testing under dependency. Ann. Stat., 29, 1165–1188, doi:10.1214/aos/1013699998.

Betts, A.K., & Harshvardhan (1987). Thermodynamic constraint on the cloud liquid water feedback in climate models. J Geophys Res 92:8483–8485

Bozkurt, D., Rondanelli, R., Marín, J. C., & Garreaud, R. (2018). Foehn Event Triggered by an Atmospheric River Underlies Record-Setting Temperature Along Continental Antarctica. Journal of Geophysical Research: Atmospheres, 123(8), 3871–3892. https://doi.org/10.1002/2017JD027796

Bracegirdle, T. J., Krinner, G., Tonelli, M., Haumann, F. A., Naughten, K. A., Rackow, T., et al. (2020). Twenty first century changes in Antarctic and Southern Ocean surface climate in CMIP6. Atmospheric Science Letters, 21(9), e984. https://doi.org/10.1002/asl.984

Catto, J. L., E. Madonna, H. Joos, I. Rudeva, and I. Simmonds (2015), Global relationship between fronts and warm conveyor belts and the impact on extreme precipitation, *J. Clim.*, *28*(21), 8411–8429, doi:10.1175/JCLI-D-15-0171.1.

Cheng, X., & Wallace, J.M. (1993). Cluster analysis of the Northern Hemisphere wintertime 500-hPa height field: Spatial patterns. J. Atmos. Sci., 50, 2674–2696, https://doi.org/10.1175/1520-0469(1993)050,2674:CAOTNH.2.0.CO;2

Cohen, L., Dean, S., & Renwick, J. (2013). Synoptic Weather Types for the Ross Sea Region, Antarctica. Journal of Climate, 26(2), 636–649. https://doi.org/10.1175/JCLI-D-11-00690.1

Copernicus Climate Change Service (C3S). (2017). ERA5: Fifth generation of ECMWF atmospheric reanalyses of the global climate. Copernicus Climate Change Service Climate Data Store (CDS), accessed february 2020. https://cds.climate.copernicus.eu/cdsapp#!/home

Dacre, H.F., Martínez-Alvarado, O., & Mbengue, C.O. (2019). Linking Atmospheric Rivers and Warm Conveyor Belt Airflows. Journal of Hydrometeorology, 20(6), 1183–1196. https://doi.org/10.1175/JHM-D-18-0175.1

Edwards, T.L., Brandon, M.A., Durand, G., Edwards, N.R., Golledge, N.R., Holden, P.B., et al. (2019). Revisiting Antarctic ice loss due to marine ice-cliff instability. Nature, 566(7742), 58–64. https://doi.org/10.1038/s41586-019-0901-4

Edwards, T.L., Nowicki, S., Marzeion, B., Hock, R., Goelzer, H., Seroussi, H., et al. (2021). Projected land ice contributions to twenty-first-century sea level rise. Nature, 593(7857), 74–82. https://doi.org/10.1038/s41586-021-03302-y

Espinoza, V., Waliser, D. E., Guan, B., Lavers, D. A., & Ralph, F. M. (2018). Global analysis of climate change projection effects on atmospheric rivers. Geophysical Research Letters, 45, 4299–4308. https://doi.org/10.1029/2017GL076968

Fauchereau, N., Pohl, B., Reason, C.J.C., Rouault, M., & Richard, Y. (2009). Recurrent daily OLR patterns in the southern Africa/southwest Indian Ocean region, implications for South African rainfall and teleconnections. Climate Dyn., 32, 575–591, https://doi.org/10.1007/s00382-008-0426-2.

Favier, V., Agosta, C., Genthon, C., Arnaud, L., Trouvillez, A., & Gallée, H. (2011). Modeling the mass and surface heat budgets in a coastal blue ice area of Adelie Land, Antarctica, J. Geophys. Res., 116, F03017, doi:10.1029/2010JF001939

Favier, V., Agosta, C., Parouty, S., Durand, G., Delaygue, G., Gallée, H., Drouet, A.-S., Trouvilliez, A., & Krinner, G. (2013). An updated and quality controlled surface mass balance dataset for Antarctica, The Cryosphere, 7, 583–597, https://doi.org/10.5194/tc-7-583-2013

Favier, V., Krinner, G., Amory, C., Gallée, H., Beaumet, J., & Agosta, C. (2017). Antarctica-Regional Climate and Surface Mass Budget. Current Climate Change Reports. https://doi.org/10.1007/s40641-017-0072-z

Fogt, R. L., & Marshall, G. J. (2020). The Southern Annular Mode: Variability, trends, and climate impacts across the Southern Hemisphere. WIREs Climate Change, 11(4). https://doi.org/10.1002/wcc.652

Gallée, H., & Pettré, P. (1998). Dynamical Constraints on Katabatic Wind Cessation in Adélie Land, Antarctica. Journal of the Atmospheric Sciences 55, 1755-1770. https://doi.org/10.1175/1520-0469(1998)055<1755:DCOKWC>2.0.CO;2>

Gelaro, R., McCarty, W., Suárez, M.J., Todling, R., Molod, A., Takacs, L., et al. (2017). The Modern-Era Retrospective Analysis for Research and Applications, Version 2 (MERRA-2). Journal of Climate, 30(14), 5419–5454. https://doi.org/10.1175/JCLI-D-16-0758.1

Genthon, C., Magand, O., Krinner, G., & Fily, M. (2009). Do climate models underestimate snow accumulation on the Antarctic plateau? A re-evaluation of/from in situ observations in East Wilkes and Victoria Lands. Annals of Glaciology, 50(50), 61-65. doi:10.3189/172756409787769735

Gillett, N., Stone, D., Stott, P. et al. (2008). Attribution of polar warming to human influence. Nature Geosci 1, 750–754. https://doi.org/10.1038/ngeo338

Goff, J.A., & Gratch, S. (1946). Low-pressure properties of water from -160 to 212F. Trans Am Soc Heat Vent Eng 52:95–121

Gorodetskaya, I. V., Tsukernik, M., Claes, K., Ralph, M. F., Neff, W. D., & Van Lipzig, N. P. M. (2014). The role of atmospheric rivers in anomalous snow accumulation in East Antarctica. Geophysical Research Letters, 41(17), 6199–6206. https://doi.org/10.1002/2014GL060881

Gorodetskaya, I. V., Silva, T., Schmithüsen, H., & Hirasawa, N. (2020). Atmospheric River Signatures in Radiosonde Profiles and Reanalyses at the Dronning Maud Land Coast, East Antarctica. Advances in Atmospheric Sciences, 37(5), 455–476. https://doi.org/10.1007/s00376-020-9221-8

Grazioli, J., Genthon, C., Boudevillain, B., Duran-Alarcon, C., Del Guasta, M., Madeleine, J.-B., & Berne, A. (2017). Measurements of precipitation in Dumont d'Urville, Adélie Land, East Antarctica, The Cryosphere, 11, 1797–1811, https://doi.org/10.5194/tc-11-1797-2017

Guan, B., & Waliser, D. E. (2015). Detection of atmospheric rivers: Evaluation and application of an algorithm for global studies: Detection of Atmospheric Rivers. Journal of Geophysical Research: Atmospheres, 120(24), 12514–12535. https://doi.org/10.1002/2015JD024257

Harrold, T. W. (1973). Mechanisms influencing the distribution of precipitation within baroclinic disturbances. Quarterly Journal of the Royal Meteorological Society, 99(420), 232–251. https://doi.org/10.1002/qj.49709942003

Hersbach, H., Bell ., Berrisford P., et al. (2020). The ERA5 global reanalysis. Q J R Meteorol Soc., 146, 1999– 2049. https://doi.org/10.1002/qj.3803

Hirasawa, N., Nakamura, H., Motoyama, H., Hayashi, M., & Yamanouchi, T. (2013). The role of synoptic-scale features and advection in prolonged warming and generation of different forms of precipitation at Dome Fuji station, Antarctica, following a prominent blocking event. Journal of Geophysical Research: Atmospheres, 118(13), 6916–6928. https://doi.org/10.1002/jgrd.50532

Huang, B., Thorne P.W., et. al. (2017). Extended Reconstructed Sea Surface Temperature version 5 (ERSSTv5), Upgrades, validations, and intercomparisons. J. Climate, doi:10.1175/JCLI-D-16-0836.1

Huth, R. (1996), An Intercomparison of Computer-Assisted Circulation Classification Methods, *Int. J. Climatol.*, *16*(8), 893–922, doi:10.1002/(SICI)1097-0088(199608)16:8<893::AID-JOC51>3.0.CO;2-Q.

Hoskins, B. J., & Hodges, K. I. (2005). A New Perspective on Southern Hemisphere Storm Tracks. Journal of Climate, 18(20), 4108–4129. https://doi.org/10.1175/JCLI3570.1

IMBIE. (2018). Mass balance of the Antarctic Ice Sheet from 1992 to 2017. Nature, 558(7709), 219–222. https://doi.org/10.1038/s41586-018-0179-y

Irving, D., & Simmonds, I. (2015). A Novel Approach to Diagnosing Southern Hemisphere Planetary Wave Activity and Its Influence on Regional Climate Variability, Journal of Climate, 28(23), 9041-9057.

Jones, D. A., and I. Simmonds (1994), A climatology of Southern Hemisphere anticyclones, *Clim. Dyn.*, *10*(6–7), 333–348, doi:10.1007/BF00228031.

Kharin, V.V., Zwiers, F.W., Zhang, X., & Hegerl, G.C. (2007). Changes in temperature and precipitation extremes in the IPCC ensemble of global coupled model simulations. Journal of Climate, 20, 1419–1444

King, J. C., & Turner, J. (2007). Antarctic Meteorology and Climatology. Cambridge University Press.

Kittel, C., Amory, C., Agosta, C., Jourdain, N. C., Hofer, S., Delhasse, A., Doutreloup, S., Huot, P.-V., Lang, C., Fichefet, T., & Fettweis, X. (2021). Diverging future surface mass balance between the Antarctic ice shelves and grounded ice sheet, The Cryosphere, 15, 1215–1236, https://doi.org/10.5194/tc-15-1215-2021

König-Langlo, G., King, J. C., & Pettré, P. (1998). Climatology of the three coastal Antarctic stations Dumont d'Urville, Neumayer, and Halley, J. Geophys. Res., 103(D9), 10935–10946, doi:10.1029/97JD00527

Lenaerts, J. T. M., Medley, B., van den Broeke, M. R., & Wouters, B. (2019). Observing and Modeling Ice Sheet Surface Mass Balance. Reviews of Geophysics, 57(2), 376–420. https://doi.org/10.1029/2018RG000622

Lenton, A., & Matear, R. J. (2007). Role of the Southern Annular Mode (SAM) in Southern Ocean CO2 uptake, Global Biogeochem. Cycles, 21, GB2016, doi:10.1029/2006GB002714

Ligtenberg, S. R. M., van de Berg, W. J., van den Broeke, M. R., Rae, J. G. L., & van Meijgaard, E. (2013). Future surface mass balance of the Antarctic ice sheet and its influence on sea level change, simulated by a regional atmospheric climate model. Climate Dynamics, 41(3–4), 867–884. https://doi.org/10.1007/s00382-013-1749-1

Liu, P. et al. (2018), Climatology of tracked persistent maxima of 500-hPa geopotential height, *Clim. Dyn.*, *51*(1–2), 701–717, doi:10.1007/s00382-017-3950-0.

Ma, W., Chen, G., & Guan, B. (2020). Poleward Shift of Atmospheric Rivers in the Southern Hemisphere in Recent Decades. Geophysical Research Letters, 47(21), e2020GL089934. https://doi.org/10.1029/2020GL089934

Madonna, E., Wernli, H., Joos, H., & Martius, O. (2014). Warm Conveyor Belts in the ERA-Interim Dataset (1979?2010). Part I: Climatology and Potential Vorticity Evolution. Journal of Climate, 27(1), 3–26. https://doi.org/10.1175/JCLI-D-12-00720.1

Marshall, G.J. (2003). Trends in the southern annular mode from observations and reanalyses. J. Climate, 16, 4134–4143

Marshall, G.J., Thompson, D.W J., & van den Broeke, M.R. (2017). The signature of Southern Hemisphere atmospheric circulation patterns in Antarctic precipitation. Geophysical Research Letters, 44, 11,580– 11,589. https://doi.org/10.1002/2017GL075998

Massom, R. A., Pook, M. J., Comiso, J. C., Adams, N., Turner, J., Lachlan-Cope, T., & Gibson, T. T. (2004). Precipitation over the Interior East Antarctic Ice Sheet Related to Midlatitude Blocking-High Activity. Journal of Climate, 17(10), 1914–1928. https://doi.org/10.1175/1520-0442(2004)017<1914:POTIEA>2.0.CO;2

McPhaden, M. J., S. E. Zebiak, and M. H. Glantz (2006), ENSO as an integrating concept in earth science, *Science (80-.).*, *314*(5806), 1740–1745, doi:10.1126/science.1132588.

Medley, B., & Thomas, E. R. (2019). Increased snowfall over the Antarctic Ice Sheet mitigated twentieth-century sea-level rise. Nature Climate Change, 9(1), 34–39. https://doi.org/10.1038/s41558-018-0356-x

Michelangeli, P.A., Vautard, R., & Legras, B. (1995). Weather regimes: Recurrence and quasi-stationarity. J. Atmos. Sci., 52, 1237–1256, https://doi.org/10.1175/1520-0469(1995)052,1237:WRRAQS.2.0.CO;2

Mottram, R., Hansen, N., Kittel, C., van Wessem, J. M., Agosta, C., Amory, C., Boberg, F., van de Berg, W. J., Fettweis, X., Gossart, A., van Lipzig, N. P. M., van Meijgaard, E., Orr, A., Phillips, T., Webster, S., Simonsen, S. B., and Souverijns, N.: What is the surface mass balance of Antarctica? An intercomparison of regional climate model estimates, The Cryosphere, 15, 3751–3784, https://doi.org/10.5194/tc-15-3751-2021, 2021.

Muller, C.J., O'Gorman, P.A., & Back, L.E. (2011). Intensification of precipitation extremes with warming in a cloud resolving model. J Clim 24:2784–2800

O'Gorman, P.A., & Schneider, E. (2009). Scaling of precipitation extremes over a wide range of climates simulated with an idealised GCM. J Clim 22:5676–5685

Pall, P., Allen, M.R., & Stone, D.A. (2007). Testing the Clausius–Clapeyron constraint on changes in extreme precipitation under CO2 warming. Clim Dyn 28:351–363

Pepler, A., A. Dowdy, and P. Hope (2019a), A global climatology of surface anticyclones, their variability, associated drivers and long-term trends, *Clim. Dyn.*, *52*(9–10), 5397–5412, doi:10.1007/s00382-018-4451-5.

Pepler, A., P. Hope, and A. Dowdy (2019b), Long-term changes in southern Australian anticyclones and their impacts, *Clim. Dyn.*, *53*(7–8), 4701–4714, doi:10.1007/s00382-019-04819-9.

Périard, C., & Pettré, P. (1993). Some aspects of the climatology of dumont D'Urville, Adélie land, Antarctica. Int. J. Climatol., 13, 313-328. https://doi.org/10.1002/joc.3370130307

Pezza, A. B., and T. Ambrizzi (2003), Variability of Southern Hemisphere cyclone and anticyclone behavior: Further analysis, *J. Clim.*, *16*(7), 1075–1083, doi:10.1175/1520-0442(2003)016<1075:VOSHCA>2.0.CO;2.

Pezza, A. B., T. Durrant, I. Simmonds, and I. Smith (2008), Southern hemisphere synoptic behavior in extreme phases of SAM, ENSO, sea ice extent, and Southern Australia rainfall, *J. Clim.*, *21*(21), 5566–5584, doi:10.1175/2008JCLI2128.1.

Pohl, B., N. Fauchereau, Y. Richard, M. Rouault, and C. J. C. Reason (2009), Interactions between synoptic, intraseasonal and interannual convective variability over Southern Africa, *Clim. Dyn.*, *33*(7–8), 1033–1050, doi:10.1007/s00382-008-0485-4.

Pohl, B., & Fauchereau N. (2012). The southern annular mode seen through weather regimes. J. Climate, 25, 3336–3354, https://doi.org/10.1175/JCLI-D-11-00160.1.

Pohl, B., Dieppois, B., Crétat, J., Lawler, D., & Rouault, M. (2018). From Synoptic to Interdecadal Variability in Southern African Rainfall: Toward a Unified View across Time Scales. J. Climate, 31, 5845–5872. doi:10.1175/JCLI-D-17-0405.1

Pohl, B., Saucède, T., Favier, V., Pergaud, J., Verfaillie, D., Féral, J.P., Krasniqi, Y., & Richard, Y. (2021a). Recent climate variability around the Kerguelen Islands (Southern Ocean) seen through weather regimes. Journal of Applied Meteorology and Climatology, in press. doi:10.1175/JAMC-D-20-0255.1

Pohl B, A Lorrey, A Sturman, H Quénol, J Renwick, N Fauchereau & J Pergaud (2021b) "Beyond Weather Regimes": Descriptors Monitoring Atmospheric Centers of Action. A case study for Aotearoa New Zealand. *Journal of Climate*, **in press**. doi:10.1175/JCLI-D-21-0102.1

Pook, M.J. (1994). Atmospheric blocking in the Australasian region in the Southern Hemisphere winter. Ph.D. thesis, University of Tasmania, 168 pp.

Pook, M.J., & Gibson, T. (1999). Atmospheric blocking and storm tracks during SOP-1 of the FROST Project. Aust. Meteor. Mag., 48, 51–60

Pook, M.J., Risbey, J.S., McIntosh, P.C., Ummenhofer, C.C., Marshall, A.G., & Meyers, G.A. (2013). The Seasonal Cycle of Blocking and Associated Physical Mechanisms in the Australian Region and Relationship with Rainfall. Monthly Weather Review, 141(12), 4534–4553. https://doi.org/10.1175/MWR-D-13-00040.1

Pook, M.J., Risbey, J.S., & McIntosh, P.C. (2012). The Synoptic Climatology of Cool-Season Rainfall in the Central Wheatbelt of Western Australia. Monthly Weather Review, 140(1), 28–43. https://doi.org/10.1175/MWR-D-11-00048.1

Pook, M. J., J. S. Risbey, and P. C. McIntosh (2014), A comparative synoptic climatology of cool-season rainfall in major grain-growing regions of southern Australia, *Theor. Appl. Climatol.*, *117*(3–4), 521–533, doi:10.1007/s00704-013-1021-y.

Ralph, F. M., Dettinger, M., Lavers, D., Gorodetskaya, I. V., Martin, A., Viale, M., et al. (2017). Atmospheric Rivers Emerge as a Global Science and Applications Focus. Bulletin of the American Meteorological Society, 98(9), 1969–1973. https://doi.org/10.1175/BAMS-D-16-0262.1

Ralph, F. Martin, Neiman, P. J., & Wick, G. A. (2004). Satellite and CALJET Aircraft Observations of Atmospheric Rivers over the Eastern North Pacific Ocean during the Winter of 1997/98. Monthly Weather Review, 132(7), 1721–1745. https://doi.org/10.1175/1520-0493(2004)132<1721:SACAOO>2.0.CO;2

Renwick, J. A. (2004), Trends in the Southern Hemisphere polar vortex in NCEP and ECMWF reanalyses, *Geophys. Res. Lett.*, *31*(7), L07209, doi:10.1029/2003GL019302.

Richard, Y., Rouault, M., Pohl, B., Crétat, J., Duclot, I., Taboulot, S., Reason, C.J.C., Macron, C., & Buiron, D. (2013). Temperature changes in the mid- and high-latitudes of the Southern Hemisphere. Int. J. Climatol., 33: 1948–1963. doi:10.1002/joc.3563

Risbey, J.S., Pook, M.J., McIntosh, P.C., Wheeler, M.C., & Hendon, H.H. (2009). On the Remote Drivers of Rainfall Variability in Australia. Monthly Weather Review, 137(10), 3233–3253. https://doi.org/10.1175/2009MWR2861.1

Risbey, J. S., D. P. Monselesan, A. S. Black, T. S. Moore, D. Richardson, D. T. Squire, and C. R. Tozer (2021), The identification of long-lived southern hemisphere flow events using archetypes and principal components, *Mon. Weather Rev.*, *149*(6), 1987–2010, doi:10.1175/MWR-D-20-0314.1.

Rutz, J.J., Shields, C.A., Lora, J.M., Payne, A.E., Guan, B., Ullrich, P., et al. (2019). The Atmospheric River Tracking Method Intercomparison Project (ARTMIP): Quantifying Uncertainties in Atmospheric River Climatology. Journal of Geophysical Research: Atmospheres, 124(24), 13777–13802. https://doi.org/10.1029/2019JD030936

Scarchilli, C., Frezzotti, M., & Ruite, P.M. (2011). Snow precipitation at four ice cores sites in East Antarctica: provenance, seasonality and blocking factors. Climate Dynamics, 37, 2107–2125. doi:10.1007/s00382-010-0946-4

Schlosser, E., Manning, K. W., Powers, J. G., Duda, M. G., Birnbaum, G., & Fujita, K. (2010). Characteristics of high-precipitation events in Dronning Maud Land, Antarctica. Journal of Geophysical Research, 115(D14), D14107. https://doi.org/10.1029/2009JD013410

Schlosser, E., Stenni, B., Valt, M., Cagnati, A., Powers, J. G., Manning, K. W., Raphael, M., & Duda, M. G. (2016). Precipitation and synoptic regime in two extreme years 2009 and 2010 at Dome C, Antarctica – implications for ice core interpretation, Atmos. Chem. Phys., 16, 4757–4770, https://doi.org/10.5194/acp-16-4757-2016

Schlosser, E., Dittmann, A., Stenni, B., Powers, J. G., Manning, K. W., Masson-Delmotte, V., Valt, M., Cagnati, A., Grigioni, P., & Scarchilli, C. (2017). The influence of the synoptic regime on stable water isotopes in precipitation at Dome C, East Antarctica, The Cryosphere, 11, 2345–2361, https://doi.org/10.5194/tc-11-2345-2017

Scott, R. C., Nicolas, J. P., Bromwich, D. H., Norris, J. R., & Lubin, D. (2019). Meteorological Drivers and Large-Scale Climate Forcing of West Antarctic Surface Melt. Journal of Climate, 32(3), 665–684. https://doi.org/10.1175/JCLI-D-18-0233.1

Seroussi, H., Nowicki, S., Payne, A. J., Goelzer, H., Lipscomb, W. H., Abe-Ouchi, A., et al. (2020). ISMIP6 Antarctica: a multi-model ensemble of the Antarctic ice sheet evolution over the 21st century. The Cryosphere, 14(9), 3033–3070. https://doi.org/10.5194/tc-14-3033-2020

Servettaz, A. P. M., Orsi, A. J., Curran, M. A. J., Moy, A. D., Landais, A., & Agosta, C., et al. (2020). Snowfall and water stable isotope variability in East Antarctica controlled by warm synoptic events. Journal of Geophysical Research: Atmospheres, 125, e2020JD032863. https://doi.org/10.1029/2020JD032863

Simmonds, I., and K. Keay (2000), Variability of Southern Hemisphere extratropical cyclone behavior, 1958-97, *J. Clim.*, *13*(3), 550–561, doi:10.1175/1520-0442(2000)013<0550:VOSHEC>2.0.CO;2.

Simmonds, I., Keay, K., & Lim, E.-P. (2003). Synoptic Activity in the Seas around Antarctica. Monthly Weather Review, 131(2), 272–288. https://doi.org/10.1175/1520-0493(2003)131<0272:SAITSA>2.0.CO;2

Sinclair, M. R. (1996), A Climatology of Anticyclones and Blocking for the Southern Hemisohere, *Mon. Weather Rev.*, *124*, 245–263.

Sinclair, V. A., & Dacre, H. F. (2019). Which Extratropical Cyclones Contribute Most to the Transport of Moisture in the Southern Hemisphere? Journal of Geophysical Research: Atmospheres, 124(5), 2525–2545. https://doi.org/10.1029/2018JD028766

Sodemann, H., & Stohl, A. (2013). Moisture Origin and Meridional Transport in Atmospheric Rivers and Their Association with Multiple Cyclones. Monthly Weather Review, 141(8), 2850–2868. https://doi.org/10.1175/MWR-D-12-00256.1

Souverijns, N., Gossart, A., Demuzere, M., Lenaerts, J.T.M., Medley, B., Gorodetskaya, I. V., et al. (2019). A new regional climate model for POLAR-CORDEX: Evaluation of a 30-year hindcast with COSMO-CLM2 over Antarctica. Journal of Geophysical Research: Atmospheres, 124, 1405– 1427. https://doi.org/10.1029/2018JD028862

Spensberger, C., M. J. Reeder, T. Spengler, and M. Patterson (2020), The connection between the southern annular mode and a feature-based perspective on southern hemisphere midlatitude winter variability, *J. Clim.*, *33*(1), 115–129, doi:10.1175/JCLI-D-19-0224.1.

Stenni, B., Scarchilli, C., Masson-Delmotte, V., Schlosser, E., Ciardini, V., Dreossi, G., Grigioni, P., Bonazza, M., Cagnati, A., Karlicek, D., Risi, C., Udisti, R., & Valt, M. (2016). Three-year monitoring of stable isotopes of precipitation at Concordia Station, East Antarctica, The Cryosphere, 10, 2415–2428, https://doi.org/10.5194/tc-10-2415-2016

Terpstra, A., Gorodetskaya, I. V., & Sodemann, H. (2021). Linking subtropical evaporation and extreme precipitation over East Antarctica: An atmospheric river case study. Journal of Geophysical Research: Atmospheres, 126, e2020JD033617. https://doi.org/10.1029/2020JD033617

Thompson, D.W.J., & Wallace, J.W. (2000). Annular Modes in the Extratropical Circulation. Part I: Month-to-Month Variability. Journal of Climate 13, 1000-1016. https://doi.org/10.1175/1520-0442(2000)013<1000:AMITEC>2.0.CO;2>

Thompson, D., Solomon, S., Kushner, P. et al. (2011). Signatures of the Antarctic ozone hole in Southern Hemisphere surface climate change. Nature Geosci 4, 741–749. https://doi.org/10.1038/ngeo1296

Tozer, C.R., Risbey, J.S., O'Kane, T.J., Monselesan, D.P., & Pook, M.J. (2018). The Relationship between Wave Trains in the Southern Hemisphere Storm Track and Rainfall Extremes over Tasmania. Monthly Weather Review, 146(12), 4201–4230. https://doi.org/10.1175/MWR-D-18-0135.1

Trenberth, K.E., Dai, A., Rasmussen, R.M., & Parsons, D.B. (2003). The changing character of precipitation. Bull Am Meteorol Soc 84:1205–1217

Turner, J., Phillips, T., Thamban, M., Rahaman, W., Marshall, G. J., Wille, J. D., et al. (2019). The Dominant Role of Extreme Precipitation Events in Antarctic Snowfall Variability. Geophysical Research Letters. https://doi.org/10.1029/2018GL081517

Udy, D. G., Vance, T. R., Kiem, A. S., Holbrook, N. J., & Curran, M. A. J. (2021). Links between Large-Scale Modes of Climate Variability and Synoptic Weather Patterns in the Southern Indian Ocean, Journal of Climate, 34(3), 883-899. https://journals.ametsoc.org/view/journals/clim/34/3/JCLI-D-20-0297.1.xml

Uotila, P., T. Vihma, A. B. Pezza, I. Simmonds, K. Keay, and A. H. Lynch (2011), Relationships between Antarctic cyclones and surface conditions as derived from high-resolution numerical weather prediction data, *J. Geophys. Res. Atmos.*, *116*(7), D07109, doi:10.1029/2010JD015358.

Uotila, P., Vihma, T., & Tsukernik, M. (2013). Close interactions between the Antarctic cyclone budget and large-scale atmospheric circulation. Geophysical Research Letters, 40(12), 3237–3241. https://doi.org/10.1002/grl.50560

Van De Berg, W., Van Den Broeke, M., Reijmer, C., & Van Meijgaard, E. (2005). Characteristics of the Antarctic surface mass balance, 1958–2002, using a regional atmospheric climate model. Annals of Glaciology, 41, 97-104. doi:10.3189/172756405781813302

Wang, Y., Ding, M., van Wessem, J. M., Schlosser, E., Altnau, S., van den Broeke, M. R., Lenaerts, J. T., Thomas, E. R., Isaksson, E., Wang, J., & Sun, W. (2016). A comparison of Antarctic ice sheet surface mass balance from atmospheric climate models and in situ observations, J. Climate, 29, 5317–5337. https://doi.org/10.1175/JCLI-D-15-0642.1

Westra, S., Fowler, H.J., Evans, J.P., Alexander, L.V., Berg, P., Johnson, F., Kendon, E.J., Lenderink, G., & Roberts, N.M. (2014). Future changes to the intensity and frequency of short-duration extreme rainfall. Rev Geophys. doi:10.1002/2014RG000464

Wille, J.D., Favier, V., Dufour, A. et al. (2019). West Antarctic surface melt triggered by atmospheric rivers. Nat. Geosci. 12, 911–916. https://doi.org/10.1038/s41561-019-0460-1

Wille, J. D., Favier, V., Gorodetskaya, I. V., Agosta, C., Kittel, C., Beeman, J. C., et al. (2021). Antarctic atmospheric river climatology and precipitation impacts. Journal of Geophysical Research: Atmospheres, 126, e2020JD033788. https://doi.org/10.1029/2020JD033788

Woollings, T., Barriopedro, D., Methven, J., Son, S.-W., Martius, O., Harvey, B., et al. (2018). Blocking and its Response to Climate Change. Current Climate Change Reports, 4(3), 287–300. https://doi.org/10.1007/s40641-018-0108-z

Zhu, Y., & Newell, R. E. (1998). A Proposed Algorithm for Moisture Fluxes from Atmospheric Rivers. Monthly Weather Review, 126(3), 725–735. https://doi.org/10.1175/1520-0493(1998)126<0725:APAFMF>2.0.CO;2

Figures & Tables

		Day_{d+1}														
		#1	**#2**	**#3**	**#4**	**#5**	**#6**	**#7**	**#8**	**#9**	**#10**	**#11**	**#12**	**#13**	**#14**	**#15**
Day_d	**#1**	**291**	129	86	73	55	71	15	93	18	17	**5**	16	31	41	66
	#2	10	**390**	67	79	9	110	3	131	2	2	**0**	3	34	48	5
	#3	7	49	**412**	110	125	7	4	84	10	**0**	**0**	5	1	17	129
	#4	7	21	47	**373**	148	69	70	46	11	4	**0**	**0**	**0**	1	8
	#5	31	**0**	57	82	**455**	7	96	39	180	8	5	4	**0**	**0**	112
	#6	23	30	3	31	12	**410**	51	125	26	93	7	**0**	23	1	3
	#7	17	**0**	1	35	59	22	**424**	5	121	95	11	**0**	1	**0**	4
	#8	83	21	11	**7**	20	23	8	**327**	129	61	154	97	94	35	89
	#9	129	**0**	6	3	78	8	79	18	**491**	81	148	80	5	1	86
	#10	91	4	**0**	1	7	75	40	38	45	**460**	108	4	46	1	2
	#11	87	2	**0**	**0**	2	**0**	2	24	52	85	**365**	141	119	9	16
	#12	93	4	11	0	2	0	0	36	26	3	51	**355**	65	173	104
	#13	38	109	3	**0**	1	36	**0**	82	**0**	13	31	36	**522**	103	1
	#14	21	126	103	3	2	**0**	**0**	50	4	**0**	4	61	30	**448**	84
	#15	79	7	153	8	101	**0**	3	61	98	**0**	15	122	4	58	**484**

Table 1. Transition between regimes, 1979-2018. The two largest (weakest) values for each regime are in dark red and red (dark blue and blue).

	SAM		ENSO	
	DJF	JJA	DJF	JJA
#1	-0.02	**0.36**	-0.17	-0.04
#2	**-0.66**	-0.14	0.15	0.14
#3	**0.64**	**0.44**	-0.07	0.00
#4	0.24	-0.06	-0.03	-0.03
#5	**0.65**	**0.37**	-0.18	-0.13
#6	**-0.57**	**-0.71**	**0.38**	-0.12
#7	-0.20	-0.30	0.01	0.02
#8	**-0.41**	-0.12	0.21	-0.04
#9	**0.58**	**0.34**	-0.22	-0.03
#10	**-0.45**	**-0.50**	0.02	-0.09
#11	-0.14	-0.23	-0.02	-0.17
#12	**0.42**	**0.37**	-0.12	-0.04
#13	**-0.69**	**-0.51**	0.25	0.14
#14	-0.05	0.16	-0.15	**0.44**
#15	**0.72**	**0.72**	-0.08	0.03

Table 2. Interannual correlations between the seasonal regime occurrences, the SAM index and the Niño3.4 index, for the austral summer (DJF) and winter (JJA) seasons, 1979-2018. Bold red (blue) cells indicate positive (negative) correlations that are statistically significant at the 95% level according to a Bravais-Pearson test.

Max_Z		vIVT	IWV
#7	$p < 10^{-4}$	63.59	69.11
	$p < 5x10^{-2}$	99.97	99.99
#9	$p < 10^{-4}$	83.76	16.98
	$p < 5x10^{-2}$	99.99	95.72
#10	$p < 10^{-4}$	99.97	98.85
	$p < 5x10^{-2}$	100.00	100.00
#11	$p < 10^{-4}$	97.31	44.76
	$p < 5x10^{-2}$	100.00	99.82
#13	$p < 10^{-4}$	0.30	0.50
	$p < 5x10^{-2}$	44.71	46.88

Table 3. For the 5 regimes most favorable to AR events, proportion (%) of samples not associated with ARs that significantly differ, at the significance level indicated in the table (p-value), from the sample of the same regime associated with ARs, in terms of maximum amplitude of geopotential height anomalies (Max_Z). Analyses are duplicated for the vIVT and IWV AR detection schemes. Samples without ARs have the same size as those with ARs and are randomly chosen among the days ascribed to the same regime. The proportion is calculated based on the corresponding 100,000 random selections of non-AR days within each regime.

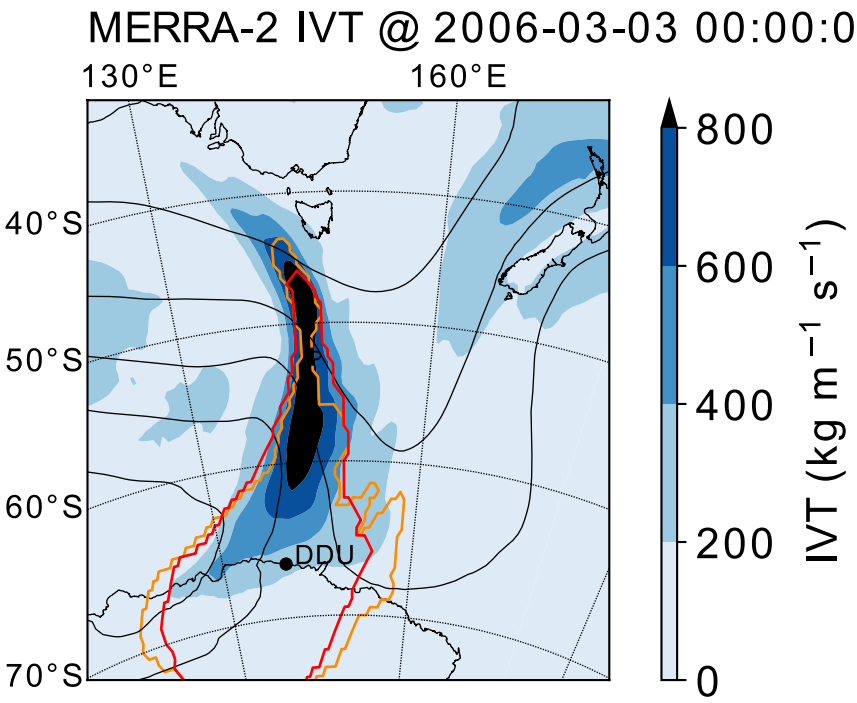

1255 **Figure 1.** Example of an AR event detected by both vIVT and IWV detection schemes on 3 March 2006. The red outline shows the delineation of the AR according to the vIVT scheme and the orange outline according to the IWV scheme. Colors represent the integrated vapor transport. Black contours show the corresponding Z700.

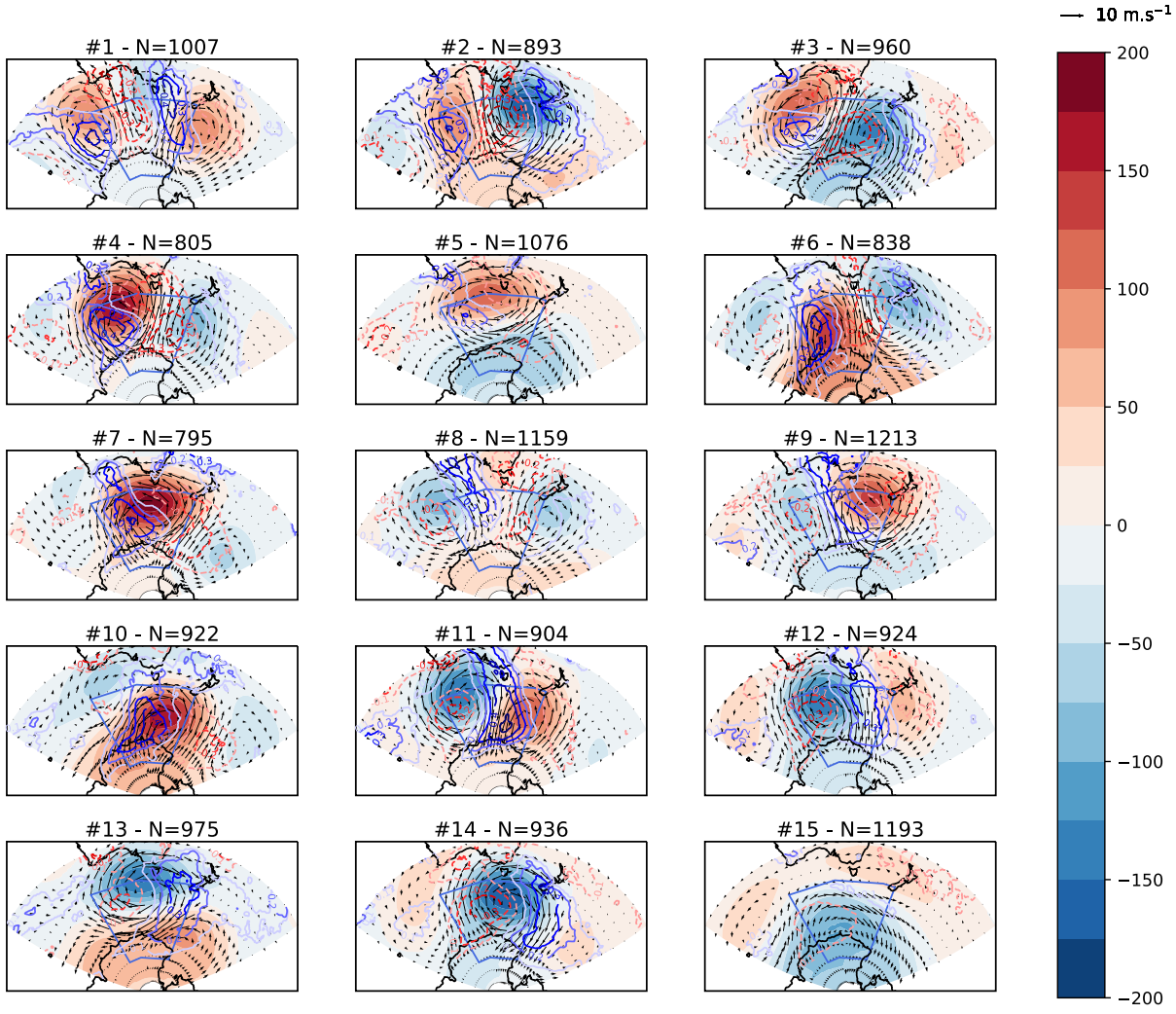

Figure 2. Anomaly patterns associated with the 15 weather regimes, period 1979-2018. Colors: Z700 anomalies (m, see color legend). Vectors: anomalies of the horizontal wind at 700 hPa ($m.s^{-1}$, see arrow key for vector scales). Contours: synchronous specific humidity anomalies at 700hPa ($g.kg^{-1}$). Contour interval is 0.05 $g.kg^{-1}$, with solid blue (dashed red) contours corresponding to positive (negative) humidity anomalies. For all variables, anomalies that are not significantly different from the mean climatology according to a t-test at the 95% confidence level are shaded white or omitted. The domain used for regime definition is shown by the inner blue polygon. N = number of days in each regime.

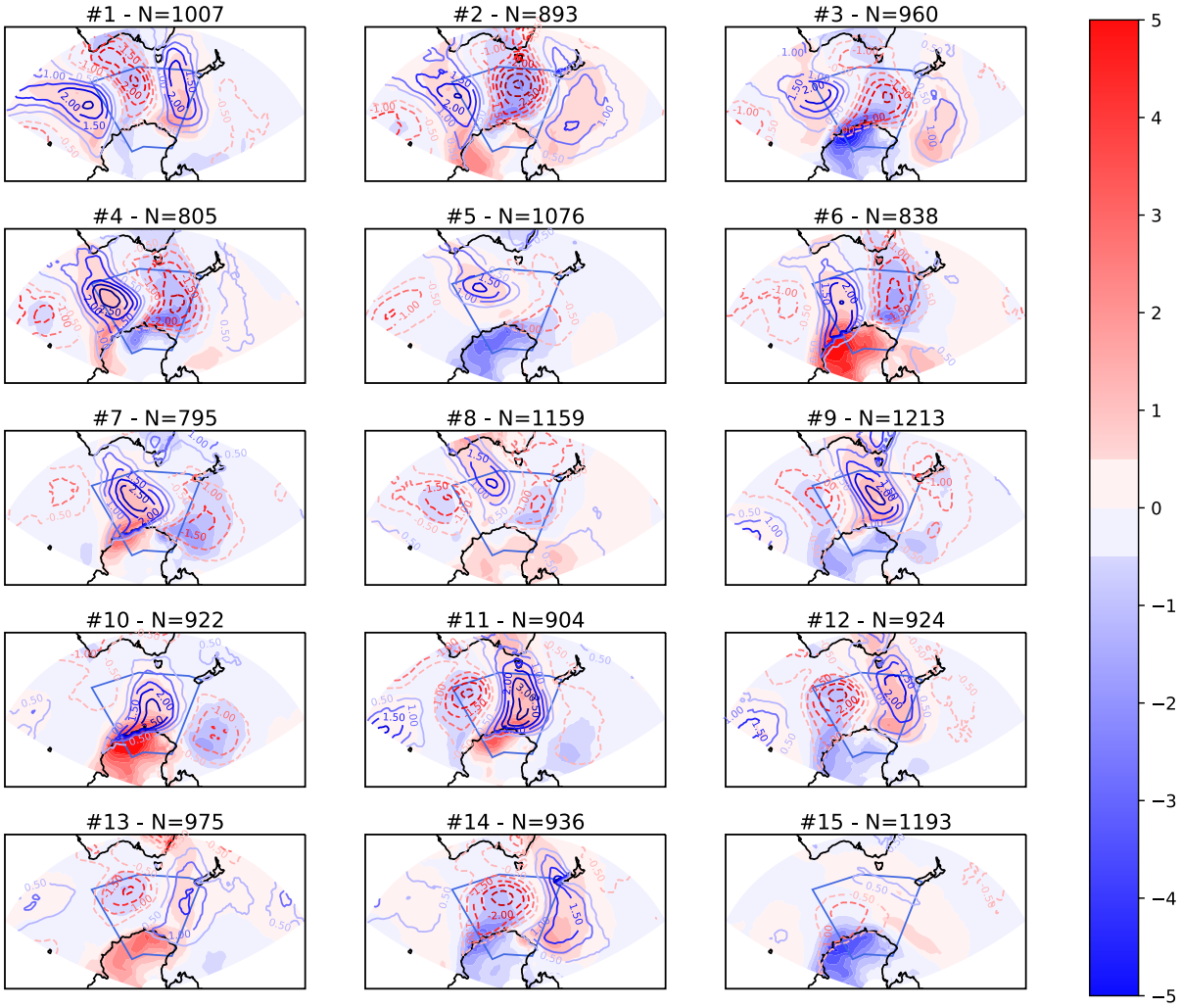

Figure 3. As Fig. 2 for the 2-m air temperature anomalies (in colors: °C, see color legend) and total column water (contours, kg.m^{-2}). Contour interval is 0.5 kg.m^{-2}, with solid blue (dashed red) contours corresponding to positive (negative) anomalies.

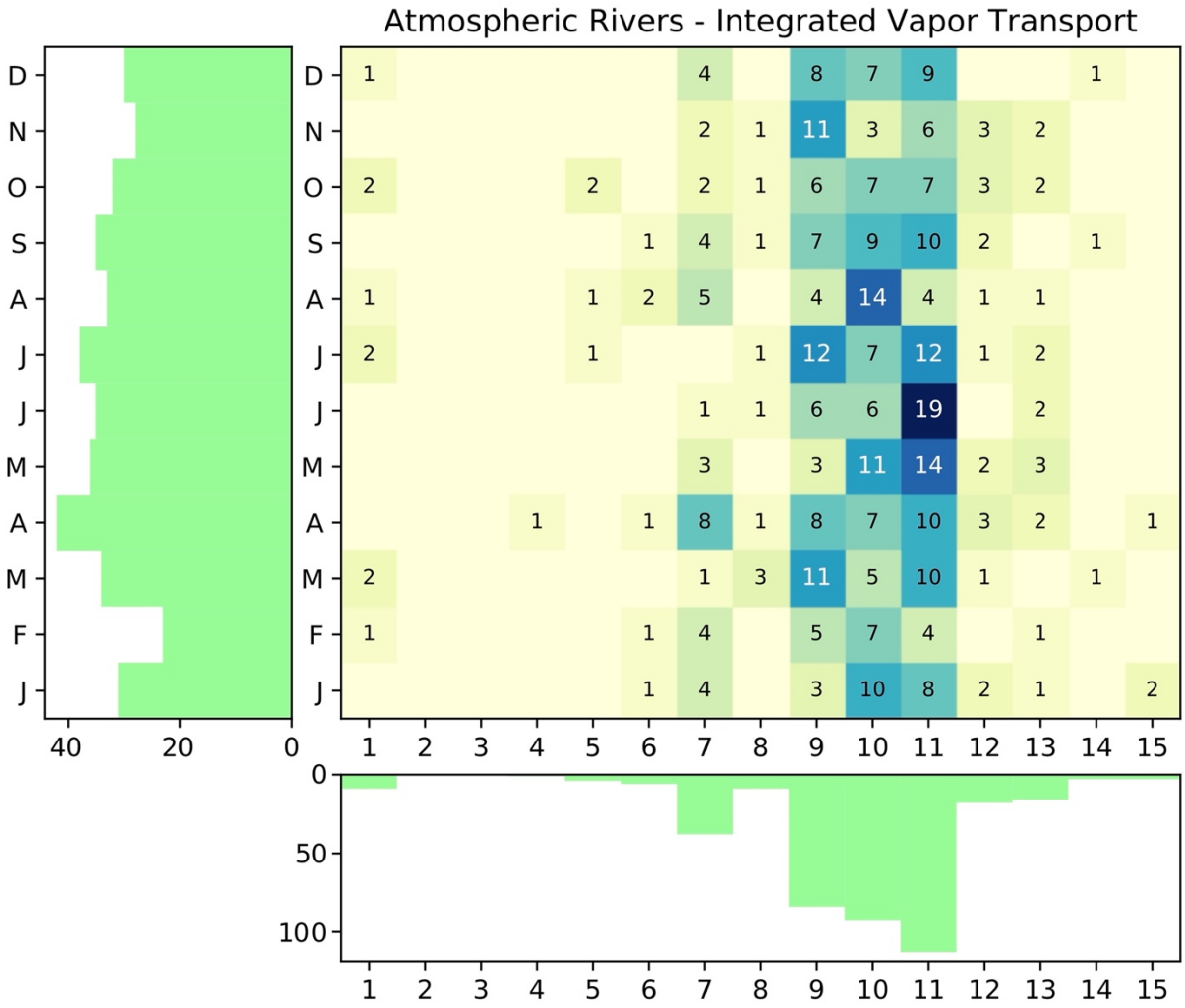

Figure 4. Time distribution of ARs (vIVT scheme: see text for details) depending on their regime (x-axis) and year (y-axis) of occurrence. The main panel indicates the average number of occurrences over the period 1979-2018. Lateral panels show the total number of occurrences per month and per regime.

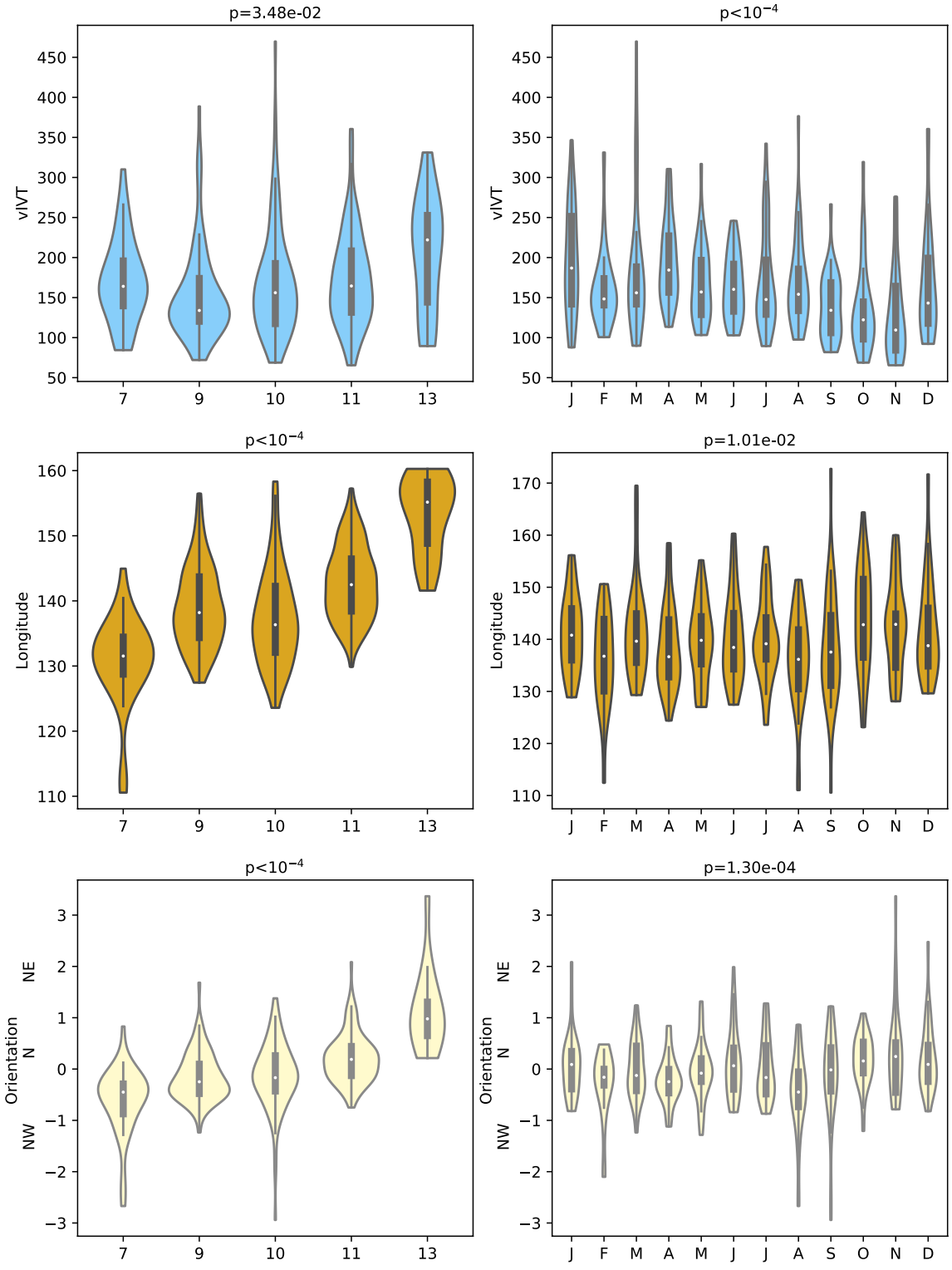

Figure 5. Violin plot of the vertically-integrated water vapor transport (first line), mean longitude (second line) and mean orientation (third line) of ARs during occurrences of the most favourable regimes (left-hand column) and over the annual cycle (right-hand column). The violin plots show the whole statistical distribution. The boxes extend from the first to the third quartile, and the white dot represents the median value. The whiskers extend to the extreme values. The significance (p-value) of an analysis of variance as estimated by a Fisher test is labeled in the figure.

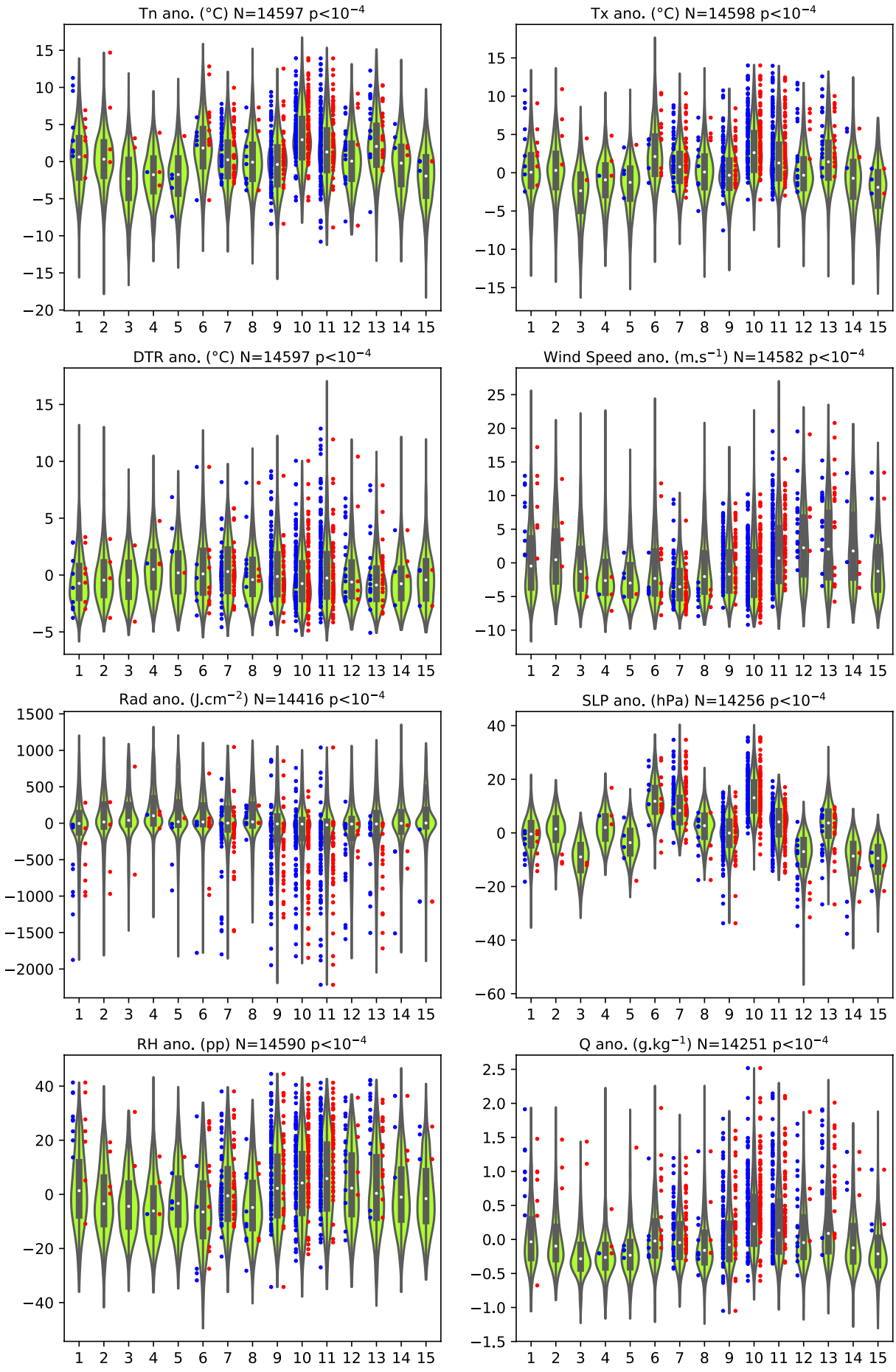
Tn ano. (°C) N=14597 p<10⁻⁴
Tx ano. (°C) N=14598 p<10⁻⁴
DTR ano. (°C) N=14597 p<10⁻⁴
Wind Speed ano. (m.s⁻¹) N=14582 p<10⁻⁴
Rad ano. (J.cm⁻²) N=14416 p<10⁻⁴
SLP ano. (hPa) N=14256 p<10⁻⁴
RH ano. (pp) N=14590 p<10⁻⁴
Q ano. (g.kg⁻¹) N=14251 p<10⁻⁴

← **Figure 6.** Composite anomalies of meteorological variables measured at the weather station of Dumont d'Urville during the regime occurrences with respect to their respective 40-yr mean climatology, period 1979-2018. Variables considered: daily minimum (Tn) and maximum (Tx) air temperature at 2m (°C); diurnal thermal range (DTR, °C); wind speed ($m.s^{-1}$); global surface radiation ($J.cm^{-2}$); sea-level pressure (hPa); relative (percentage points) and specific humidity ($g.kg^{-1}$). The number of data included in each analysis is labeled in each panel title. Violin plot representation, sample construction and statistical significance are as in Fig. 5. The blue (red) dots represent days associated with ARs as detected by the vIVT (IWV) scheme.

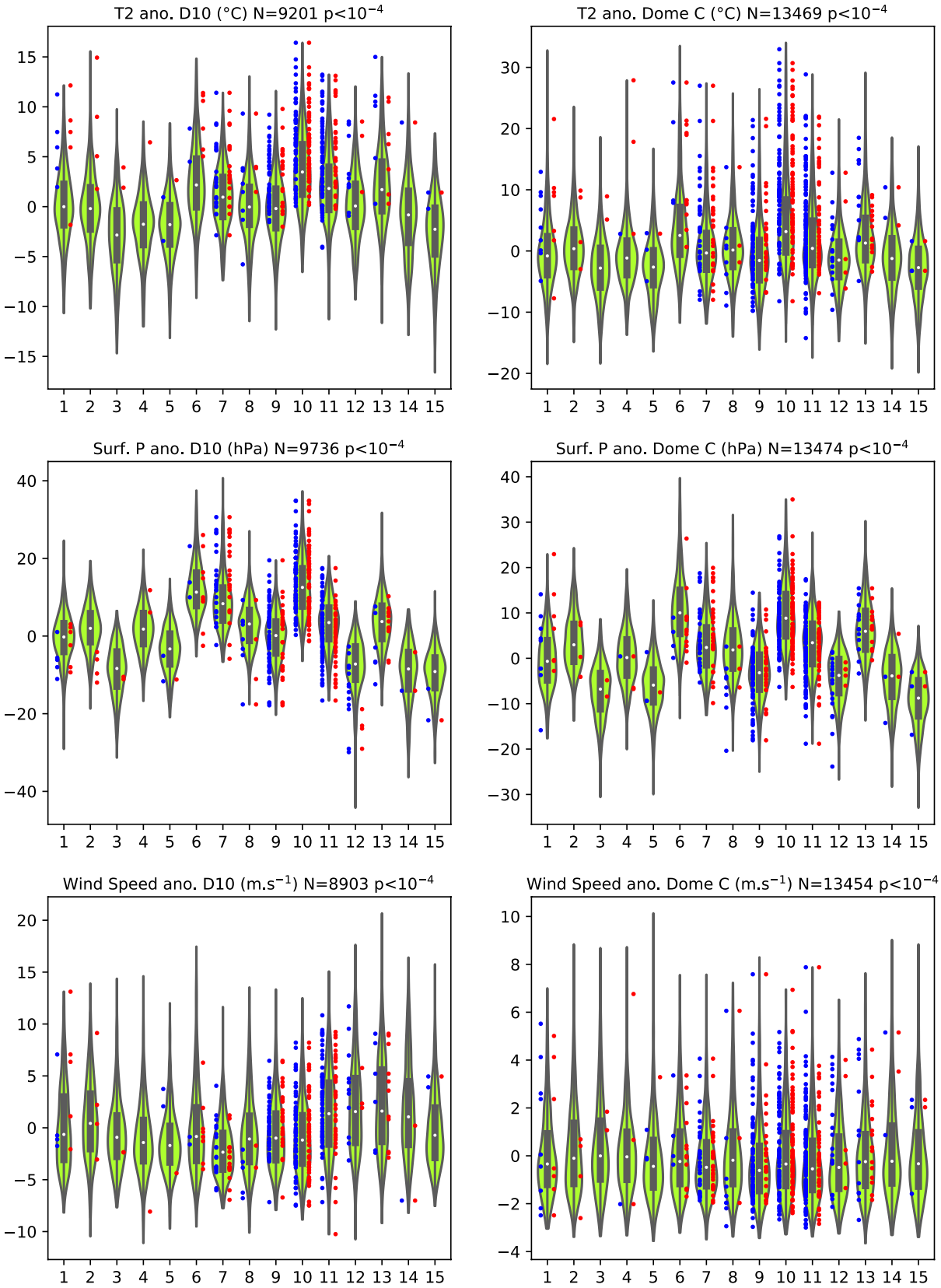

1310 **Figure 7.** As Fig. 6 but for a comparison between the automatic weather stations of Antarctica coastline (D10, left-hand column) and hinterland (Dome C, right-hand column). Location of stations is shown in Fig. 8.

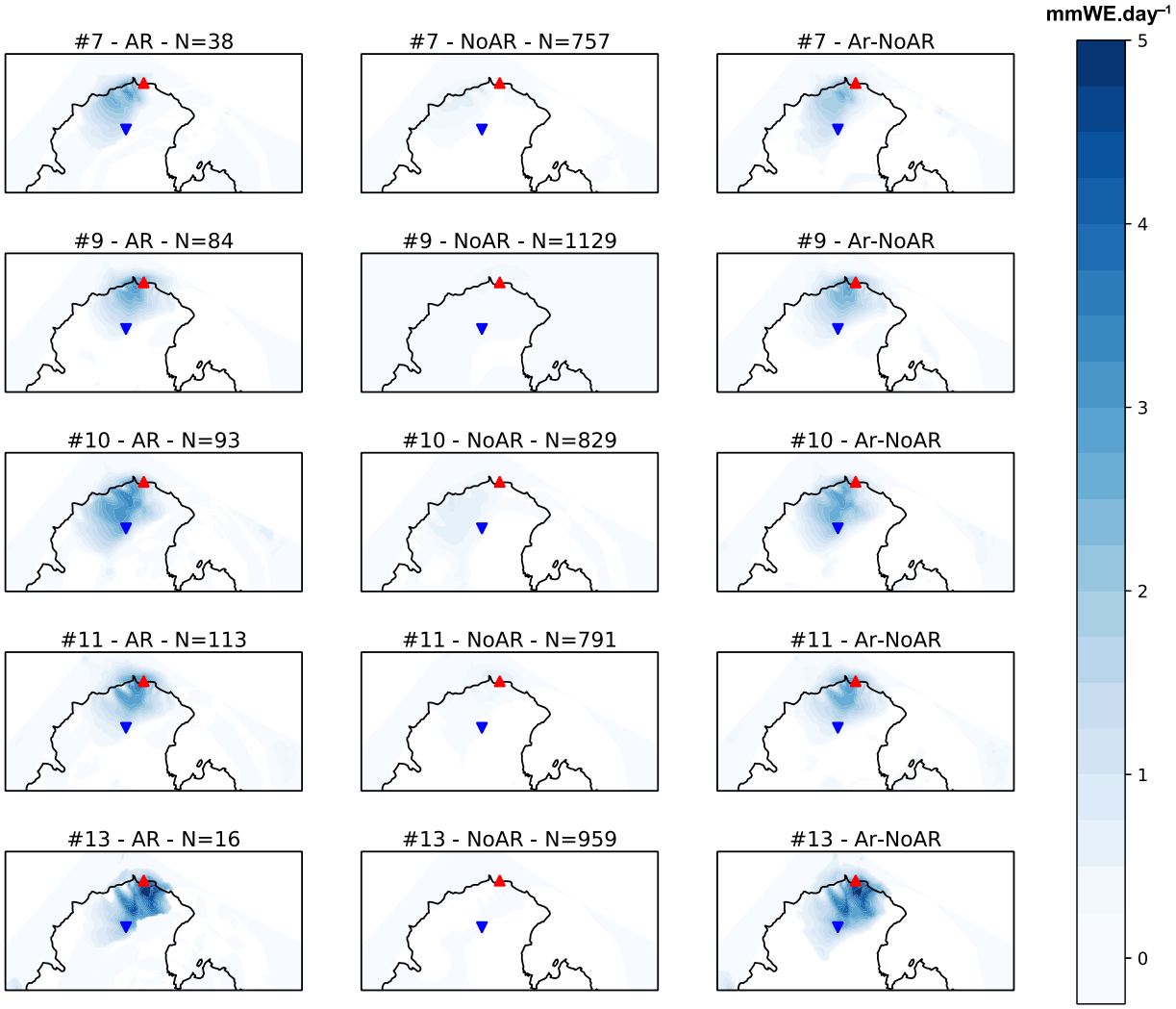

Figure 8. Simulated anomalies of daily mean snowfall accumulation (mmWE.day^{-1}, see color legend) for selected regimes associated with largest AR occurrences (Fig. 3), during AR occurrences (left-hand column), without AR occurrences (central column), and differences between both samples (right-hand column). Significance of anomalies for the first two columns is tested as for Figure 2, while the differences between samples is tested using a two-tailed t-test (right-hand column). The red (blue) triangle shows the location of the Dumont d'Urville (Dome C) station. Anomalies that are not significantly different from the mean climatology according to a t-test at the 95% confidence level are shaded white. N = number of days in each regime.

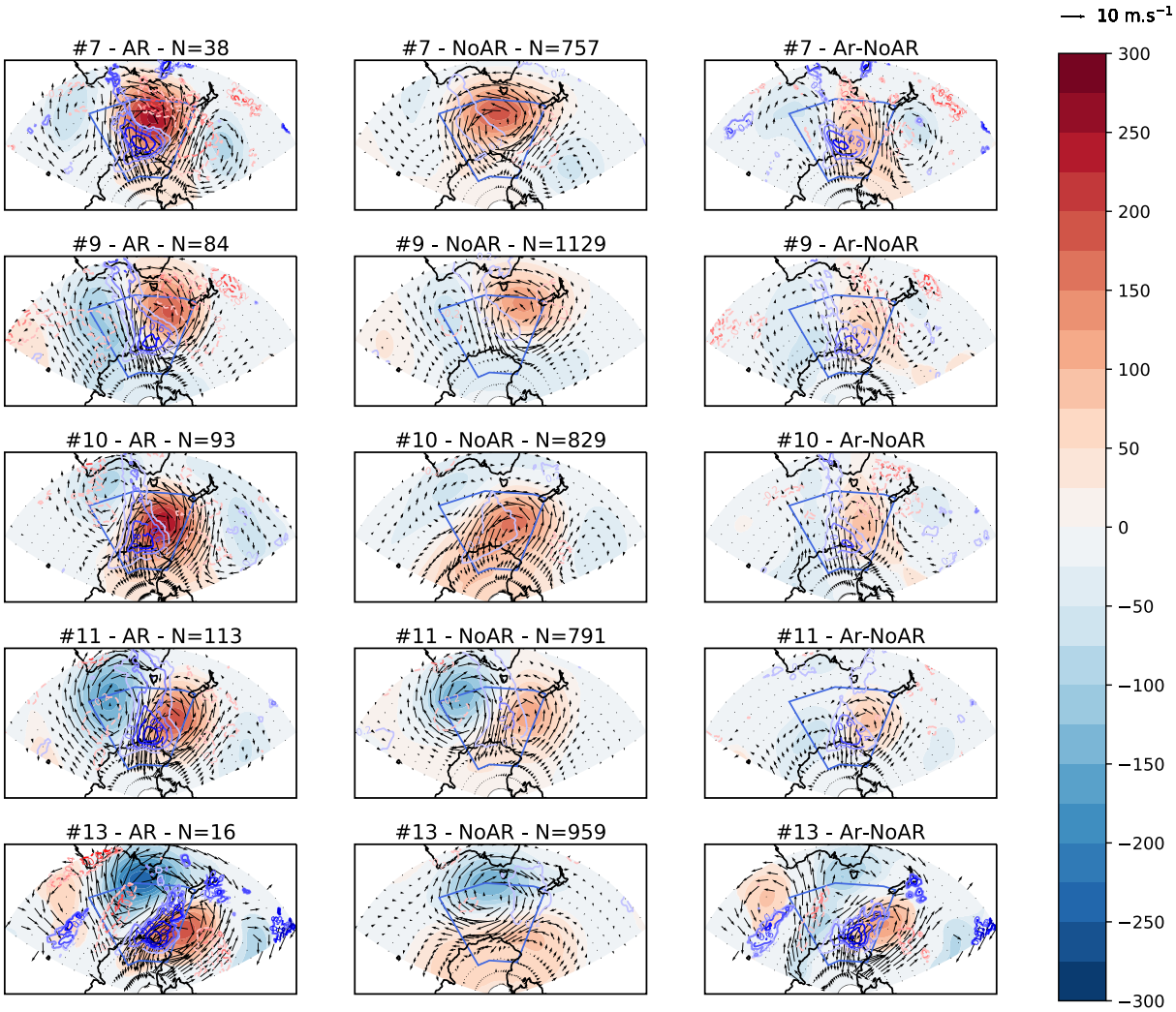

Figure 9. As Figure 2 but for selected regimes associated with largest AR occurrences (Fig. 4), during AR occurrences (left-hand column), without AR occurrences (central column), and differences between both samples (right-hand column). Significance of anomalies and differences between samples tested as in Fig. 8.

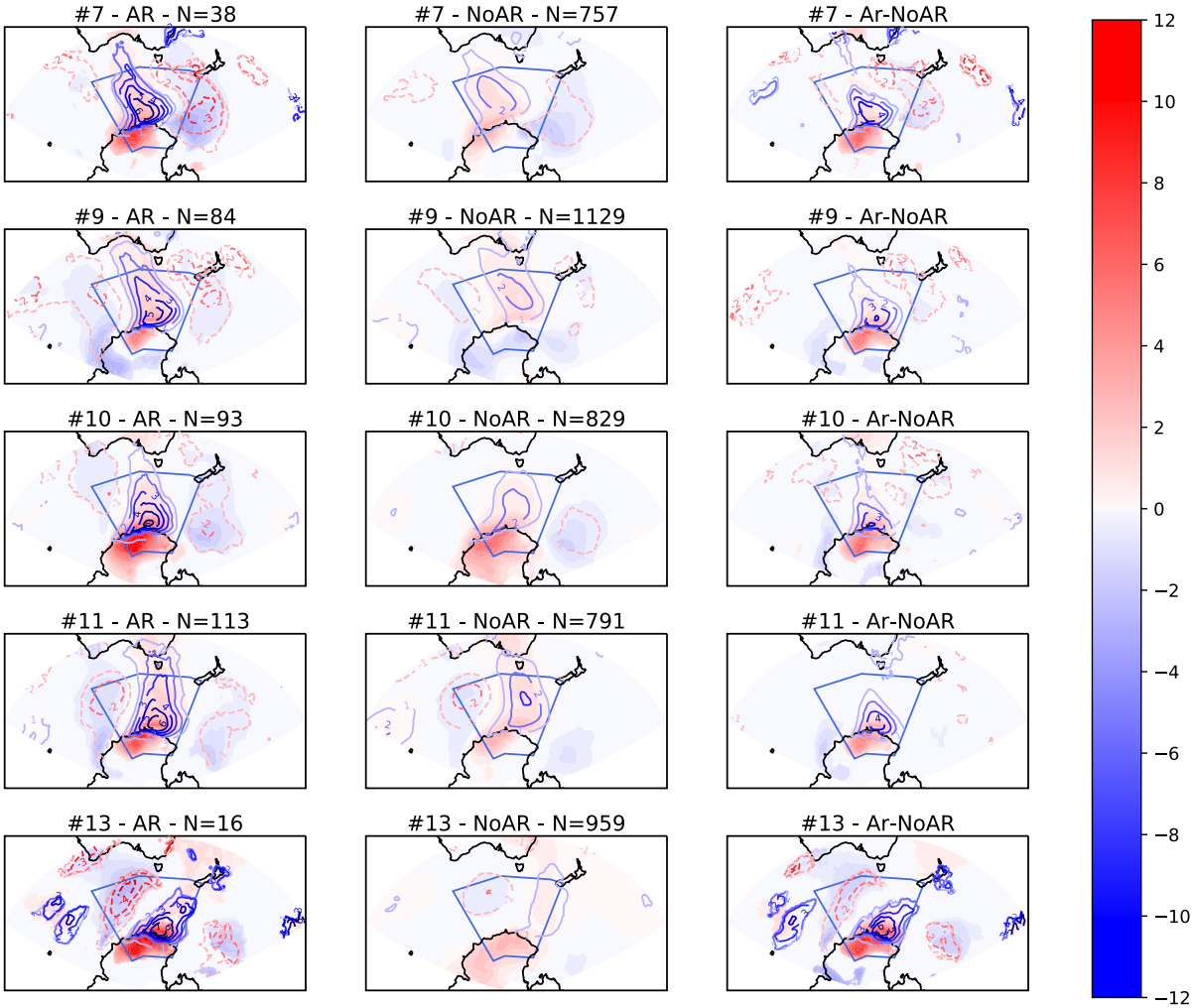

Figure 10. As Figure 3 but for selected regimes associated with largest AR occurrences (Fig. 4), during AR occurrences (left-hand column), without AR occurrences (central column), and differences between both samples (right-hand column). Significance of anomalies and differences between samples tested as for Fig. 8.